Study of Deep Drawing Process and its Parameters Using Finite Element Analysis

A DISSERTATION

SUBMITTED IN PARTIAL FULFILLMENT OF THE REQUIREMENTS FOR THE AWARD OF THE DEGREE

OF

MASTER OF TECHNOLOGY

IN

PRODUCTION ENGINEERING

Submitted by

Srijan Bansal

2K20/PIE/08

Under the supervision of

Dr. Vijay Gautam

Professor

(Mechanical Engineering Department)

DEPARTMENT OF MECHANICAL ENGINEERING

DELHI TECHNOLOGICAL UNIVERSITY

(Formerly Delhi College of Engineering)

Bawana Road, Delhi-110042

MAY, 2022

CANDIDATE'S DECLARATION

I, **Srijan Bansal**, Roll No. **2K20/PIE/08** of M.Tech. (Production Engineering), hereby certify that the project Dissertation titled "**Study of Deep Drawing Process and its Parameters Using Finite Element Analysis**" which is submitted by me to the Department of Mechanical Engineering, Delhi Technological University, Delhi in partial fulfilment of the requirement for the award of the degree of the Master of Technology is original and not copied from any source without proper citation. This work has not previously formed the basis for the award of any Degree, Diploma Associateship, Fellowship, or other similar title or recognition.

Place: Delhi

Date:

Srijan Bansal

2K20/PIE/08

M.Tech (Production Engineering)

Delhi Technological University

CERTIFICATE

I hereby certify that the Project Dissertation titled "**Study of Deep Drawing Process and its Parameters Using Finite Element Analysis**" which is submitted by **SRIJAN BANSAL** 2K20/PIE/08, Mechanical Engineering Department, Delhi Technological University, Delhi in partial fulfilment of the requirement for the award of the degree of Master of Technology, is a record project work carried out by the student under my supervision. To the best of my knowledge this work has not been submitted in part or full for any Degree or Diploma to this University or elsewhere.

Place: Delhi

Date:

Dr. VIJAY GAUTAM

SUPERVISOR

Professor

Department of Mechanical Engineering

Delhi Technological University

ACKNOWLEDGEMENT

First of all, I wish to convey my deep gratitude and sincere thanks to my M.Tech supervisor, **Prof. Vijay Gautam** for allowing me to pursue this research work at Delhi Technological University. I feel very fortunate that I got an opportunity to work under his supervision.

Besides my supervisor, I would also like to thank the following:

To my senior, **Subhajit Konar** for being present during the best and the worst moments of this journey. All the confusion, doubts, and sleepless nights became easier because of him.

To **Dr. Ved Prakash**, for his continuous support and guidance which helped me to attain the right direction

To **Bijendra Prasad,** for explaining various topics, imparting knowledge, and clearing doubts.

To my **parents** for their constant support and belief in me, even more than I do. They are the biggest source of motivation in my life.

Finally, I like to thank each and every person who was involved directly or indirectly in helping me to successfully complete this project.

SRIJAN BANSAL

2K20/PIE/08

M.Tech. (Production Engineering)

Delhi Technological University

ABSTRACT

Deep drawing is a sheet metal forming process in which a flat blank is deformed to form cylindrical cups. It is a widely popular technique in the automobile, aerospace, and packaging industries. A considerable amount of study has been already done in this field, but there is still a huge scope for further exploration.

The objective of this research work was to demonstrate the overview and to study the various parameters influencing the drawability of the deep drawing process. The quality and drawability of deep-drawn products majorly depend upon parameters such as blank position, speed, sheet thickness, clearances, coefficient of friction between die-sheet and punch-die, blank holding force, strain rate, temperature, etc. For this purpose, the deep drawing process was modelled and simulated in Ls-Dyna PrePost (R) V4.6.17 finite element analysis software. AA6082-T6 material was taken into consideration which was later annealed to attain higher elongation. Further, to predict the accurate material behaviour for the AA6082 Barlat-3 parameter anisotropic yield criterion was utilized. The Barlat material parameters and constants were determined by the tensile and anisotropy test.

The results revealed that annealing increased elongation by 15% which was earlier in the range of 4-5%. The thickness in the flank region was increased as it experiences two opposite natures of stress. Additionally, as the sheet thickness decreased, there was an increase in blank holding force which was required to remove wrinkling. With the rise in coefficient of friction, there was a decrease in sheet thickness at the wall section. It was concluded that LDR increases with an increase in sheet thickness, coefficient of friction between punch and sheet, and die radius. Thinning resistance is more in isotropic material as compared to anisotropic materials which will eventually lead to deeper cups Also, LDR decreases with an increase in punch speed, blank holding force, friction between die and sheet, and punch radius. The deep drawing model also experiences high strain rates at a certain temperature during the process which is not taken into consideration during the Barlat model. Thus, to predict the combined behaviour of strain, strain rate, and temperature Johnson-Cook model is used for material characterization.

Keywords: *Limiting Draw Ratio (LDR); Barlat-3 parameter model; Johnson-Cook model; AA6082; Ls-Dyna; Blank Holding Force (BHF)*

TABLE OF CONTENTS

Chapter 4: RESULT AND DISCUSSION

Chapter 5: CONCLUSIONS

REFERENCES

ABBREVIATION

D_{max}	Maximum diameter of the blank
D	Diameter of punch
P	Force,
A	Area of the test specimen
σ_y	Yield stress of a material in tensile test
Σ	Stress experienced by a material
σ_x , σ_y , σ_z , σ_1 , σ_2 , σ_3	Normal stress in x,y,z direction
τ_{xy},τ_{zy}, τ_{xz}	Shear stress in x, y,z direction
F, H,G,N,L,M	Anisotropic constants
FLD	Forming Limit Diagram
σ_b	Yield stress in biaxial stress
M	Non-linear relationship coefficient
a, c, h, p, m	Material parameters
σ_y	Yield stress
K_1,K_2 , K_3	Principle deviatoric Stress
ε_w	Width strain
ε_t	Thickness strain
d_{2minor}	Minor diameter of the ellipse
d_{2major}	Major diameter of the ellipse
σ_e	Engineering stress
ε_e	Engineering strain
F	Force applied
A_o	Initial area of cross-section of the specimen
, ΔL	Changes in length
L_o	Original gauge length of the specimen.
N	Strain hardening exponent
K	Strength coefficient
A	Yield stress under reference deformation conditions
B	Strain hardening constant
C	Strain rate strengthening coefficient
M	Thermal softening coefficient

T_{ref}	Reference temperature
T_m	Melting temperature
$\dot{\varepsilon}^*$	Dimensionless strain rate
T^*	Homologous temperature
$\dot{\varepsilon}_{ref}$	Reference strain rate
ε_p^n	Equivalent plastic strain
μ	Poisson ratio
P	Mass Density
σ_e	Equivalent stress
σ_ϕ	Uniaxial tension in the ϕ direction.
σ_{UTS}	Stress at ultimate tensile stress
E	Shear modulus
C_p	Specific heat

LIST OF FIGURES

LIST OF TABLES

CHAPTER 1

INTRODUCTION

1.1. GENERAL

The metal forming process is being around us for centuries. Copper was subjected to a metal forming process in early 4500BC when it was hammered with stones. The steel was forged in a metallurgical furnace in late 1000BC to yield steel [1], [2]. In the 7th century, coins were die-forged in the Greek region made up of silver giving another impression of metal forming. Then with the advancement of technology water-powered rolling mills were used, which ultimately lead to sheet forming for large ships. The greatest invention is the engine resulted in further inventions and technologies like a steam hammer, hydraulic press, continuous rolling bed, and many more. Now in the twentieth-century metal forming is of utmost importance for automobiles, aerospace, and other essential industries to produce structures, components, and parts[2]

Metal forming process is defined as a mechanical process in which the starting material (blank or workpiece) transforms its form (shapes and sizes) by the application of stresses such as tension, shear, and compression depending on the requirement to attain the shapes of a wire, plate, or sheets. The form of the material changes without removing the material nor adding the material and also mass is constant[3]. The required stress surpasses the yield strength of a material, as the material undergoes a plastic-type of deformation. There is no material removal and only the shape of the material is deformed. Metal forming processes include spinning, rolling, deep-drawing, stretching, bending, etc [4].

Sheet metal forming is a widely utilized metal forming process nowadays[5]. In the sheet metal process, the load is applied to a material to alter its geometry and form a sheet rather than removing any metal. As it deforms plastically, it is easier to bend and stretch according to the desired shape by applying the required forces. Sheet metal forming has various processes like bending, roll-forming, spinning, deep-drawing, and stretch-forming. Sheet metal forming finds application in automobiles, aerospace, and household utensils because of its high productivity and strength[6]. The various parameters influencing sheet metal forming are punch speed, blank holding force (BHF), die radius, and material properties[7].

The properties which affect the sheet metal forming are strain hardening exponent, anisotropy, and thickness of the sheet material [8]. Strain hardening exponent (n) tells us the capability of distribution of strain when we are stretching the material in tension. Forming limit of a material improves with the increment in the strain hardening exponent and it has the most impact on the right side of FLD. The biaxial tension region becomes small if we decrease the strain hardening exponent by cold working[9]. Therefore, the strain hardening exponent decreases with cold working and in turn reduces formability. Anisotropy is the ratio between the true strain of width ε_w in a material to the true strain of thickness ε_t.The drawability of material and earring is affected by the normal anisotropy ($\overline{R}$) and planar anisotropy (ΔR) during deep drawing. Higher formability is achieved at higher thickness[10]. At the neck, we have large strain because of the greater thickness of sheet metal. The strain rate sensitivity index (m) is responsible for the shape of the neck. If we have a smaller m value the neck would be steeper. With a steeper neck, there would be minimal impact on the thickness.

The constitutive equation of a flow curve is given by the reading of load versus elongation data. At a particular material microstructure and flow direction the equation of flow curve is the function of strain (ε), strain rate ($\dot{\varepsilon}$) and temperature (T)[8]. Flow curve is expressed as given in equation 1:

$$\sigma_f = f(\varepsilon, \dot{\varepsilon}, \mathrm{T}) \qquad (1)$$

1.2. DEEP DRAWING PROCESS

Deep-drawing is a well-known sheet-metal forming process in which a flat sheet is drawn radially into a circular die to form a hollow component by the operation of a punch[11]. It is referred to as a deep drawing process since the drawn dept will be more than the diameter of the circular sheet. The deep-drawing process is shown in Figure.1 a) and their various parts are marked and defined. In Figure.1 b) mechanism and working of the deep-drawing process are visualized in detail. This process has numerous advantages and applications in automobiles as components of parts, aerospace, kitchenware as utensils, domestic gas cylinders, and packaging industries.

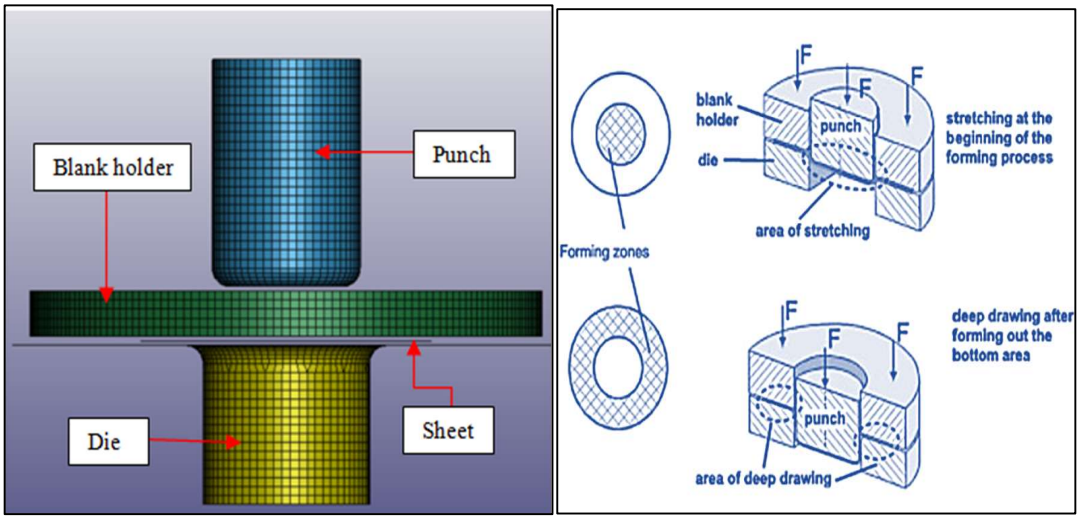

Figure.1 a) Deep-drawing parts b) Forming zones and forming areas in the deep-drawing process [12]

The various parts of the deep-drawing process are tools such as punch, die, sheet, and blank holder. The punch is a cylindrical body with a flat bottom and a slight curve at the edges called punch profile radius. Die has a circular hole with a die profile radius which is used to give shape to the sheet; circular dies give cup-sized shapes for instance. The blank holder is a circular body with a load at the upper surface to hold the sheet intact with the die. The blank sheet which is placed in between the die and the blank-holder has a diameter more than the diameter of the die hole. The sheet is deformed by the action of punch pushing it against the frictional forces. After that sheet bends and slides over the surface of the die profile radius and then eventually takes the shape of the die it is been pushed into[13].

To study the mechanism of deformation, the blank in the deep drawing process can be divided into X, Y, and Z regions as shown in Figure.2 below which will help us understand the working a little better. Region 'X' is clubbed between the blank holder from the top and the die at the bottom. Region 'Y' is free from both sides and region 'Z' is only in contact with the punch from the top. The compressive force is applied by the punch, and the punch progresses downward towards the sheet and pushes it into the die cavity radially inwards. The material in region 'X' is pulled towards the cavity which results in thinning of sheets in this region from the inner circumference[14]. A blank holding load is applied on the blank holder which controls the flow of material and prevents wrinkling [15].

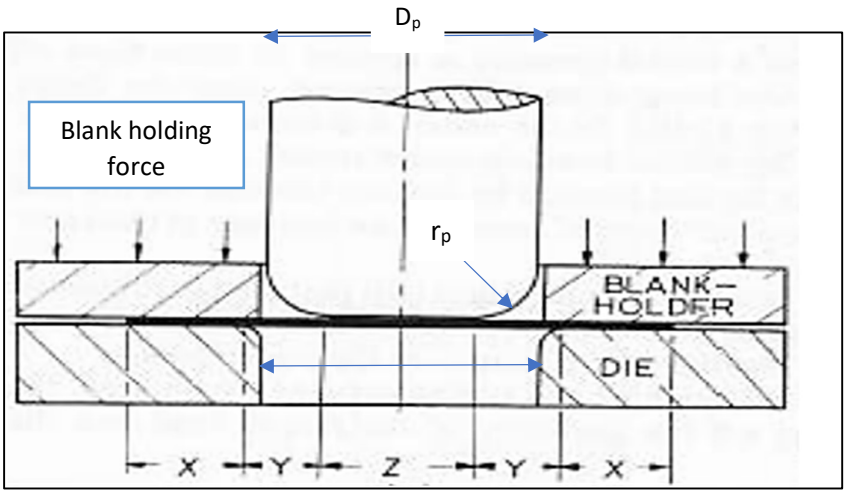

Figure.2 Deep Drawing working[14]

1.2.1. Stress in circular deep drawing

The stress in the deep-drawing is the combined effect of all these processes: - [16]

i. Drawing the flange against friction between the die and blank holder.

ii. Bending of the sheet at the punch profile radius.

iii. Bending of the sheet at the die profile radius.

iv. Slipping of the sheet over the die profile radius

v. Unbending of the sheet to a cup wall surface

To determine the stresses in the deep drawing process, we will consider a pie-shaped region as shown in Figure.3 from the actually drawn cup. The stress zones we are interested in are the flange region, cup wall region, and bottom region. All these stress zones are responsible for variation in thickness in a deep-drawn cup. The deformation in the flange region occurs because as the punch advances the adjoining sheet pulls the sheet into the die against friction. Therefore, the flange region experiences two opposite natures of stress namely hoop or circumferential stress and radial stress. So, the nature of the load is tensile in the radial direction and compressive in the circumferential direction. As a result, thickness in the area flank region increases [17].

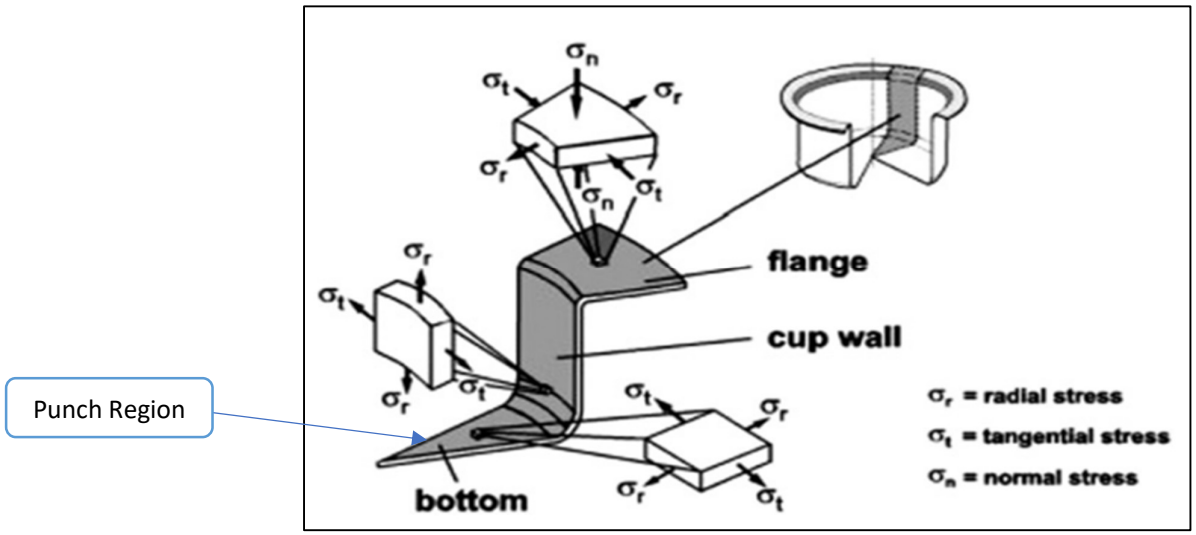

Figure.3: Stress-conditions in a drawn cup[12]

The second zone of deformation is the transition between the cup wall and the punch profile radius. The region undergoes uniform axial stretching which will lead to thinning in this portion and therefore be characterized as plane strain load. The deformation in the cup bottom is a result of a biaxial stress load. As a result of this biaxial stress, it will lead to stretch forming[12], [17].

1.2.2. Design guidelines for deep drawing

The design specification for deep drawing is mentioned below[18]:

- The die radius must be '10' times that of the thickness of sheet.
- The punch radius must not be small to avoid thinning
- The punch-die clearance the must be greater than '20 - 40 %'of sheet thickness.
- The die side must be lubricated to avoid friction

1.2.3. Parameters affecting the deep drawing process

1.2.3.1. Blank holding pressure

The pressure/load applied by the blank holder on the blank in order to lock the sheet between the die and blank holder is called **Blank holding pressure.** Blank holding pressure is mainly

used to minimize wrinkling. There should be an optimal level of the value of blank holding r pressure. If the value is too large it will lead to necking and tearing or if the value is too low wrinkles are forms on the flank or wall of the drawn sheet. Therefore, many researchers are optimizing the blank holding pressure to an optimal level.[19]

Amit Jaisingh et al.[20] found that thinning strain is affected the most because of blank holding force. After thinning, the parameters which are affected are coefficient of friction, plastic strain ratio, and strain hardening

Generally, blank-holding pressure that is normally used is of one of the two types, clearance blank-holding, and pressure blank-holding. Blank-holding pressure's main objective is to avert wrinkling with the condition to not interfere with the usual deep drawing process. Initial clearance of 5% is satisfactory in mild steel with clearance blank-holding. For pressure blank holding 400 psi of pressure on a blank area is sufficient to avert wrinkling. Surpassing this pressure had no or minimal impact on the thickness of the final cup or the maximum load of the punch but at higher loads thinning is increased.[8]

1.2.3.2. Drawing ratio

The drawing ratio is described as the ratio of the diameter of the blank to the diameter of the throat of the die. Approximately linearly, punch load increases with the blank diameter for any of the drawing conditions over a wide range with a drop at the region around LDR[21].

Limiting draw ratio (LDR) in simple terms is the mathematical ratio of the maximum diameter of the blank to the punch diameter after a deep-drawing operation as shown in equation 2. The diameter of the cup should be such that it should not fail and be safely drawn without tearing[22]. The LDR is a great tool to classify material formability or drawability. Formability increases with increases in LDR and decreases within decrease in LDR[23]. LDR is a material property but the drawing ratio is a geometrical parameter.

$$\text{LDR} = \frac{D_{max}}{d} \qquad (2)$$

Where, 'D_{max}' is the maximum diameter of the blank and 'd' is the diameter of punch

1.2.3.3. Radial clearance between punch and die

The clearance between the die and punch should be sufficient to avoid ironing. In ironing, if the clearance is less than the thickness of the sheet of the part it gets thickened then there is

rubbing or ironing which will eventually lead to uniform thickness of the sheet. In ironing the punch force is increased [24].

1.2.3.4. Die profile radius

With the increase in the die profile radius, it is seen that the maximum drawing force also tends to decrease. There is an overall increase in the maximum punch load if there is a sharper die profile radius. There will be a decrease in LDR if the die profile radius turns out to be below 15 times that of blank thickness. It is seen that there will be a steep rise in punch load and punch travel if there will be more than expected increase in punch radius. [8]

1.2.3.5. Punch profile radius

As we know that, fracture in a cup drawing occurs at the punch profile radius so this profile is the most important parameter to carefully choose [14]. The wall of the cup gets work-hardened because of the bending and unbending of the sheet hence the walls are strengthened. But on the other hand, punch profiles don't undergo work hardening as in the case of cup. Thinning increases as the punch profile radius increases.[8]

1.2.3.6. Anisotropy

The study of the microstructure of a material is very essential as it determines the formability of the material. We have either isotropic material whose properties are the same in all directions else we have anisotropic material where the properties of a material change in various directions[3]. The anisotropic material can be of two types that is, a) Normal anisotropy and b) Planer anisotropy. Normal anisotropy measures the properties of the material which varies in thickness of material whereas Planer anisotropy measures the properties of the material which varies in the plane of the material [25]. The direction in which we roll the material i.e., the rolling direction is the predominant reason for planer anisotropy. The grains of a material elongate in the rolling process which leads to different properties in different directions. The grains align in the rolling direction and the remaining got a pack in the thickness direction. As a result of aligning and packing of material, the microstructure of a material has different directions in the rolling direction and transverse or perpendicular direction. [8]

Plastic strain ratio is the ratio of the width of true strain to the thickness of true strain as given in Equation (3) and it has the ability to resist thinning when the material is under the action of uniaxial tension or compression. The material is said to be isotropic if the r value is 1. It is also

found the high r is desirable as the high value of r resists thinning. So if we have a low r-value, it will neck early and fail [8].

$$r = \frac{\varepsilon_w}{\varepsilon_t} \tag{3}$$

Where,

R	Plastic strain ratio or Lankford coefficient
ε_w	Width strain
ε_t	Thickness strain

These plastic ratios are determined in the rolling, diagonal, and transverse directions as r_0 , r_{45} and r_{90} and these are also referred to as Lankford coefficients.

Normal anisotropy can be calculated from strain ratios as given in Equation (4)

$$r_m = \frac{r_0 + 2r_{45} + r_{90}}{4} \tag{4}$$

Where,

r_m	Normal Anisotropy
r_0	Strain ratio in rolling or 0° direction
r_{45}	Strain ratio in 45° direction of rolling direction
r_{90}	Strain ratio in 90° direction of rolling direction

Planer anisotropy can be defined from the strain ratios as given in the Equation (5)

$$\Delta r = \frac{r_0 - 2r_{45} + r_{90}}{2} \tag{5}$$

Where, Δr represents planer anisotropy in Equation (5)

Planer anisotropy is used whenever we talk about earing tendency.

1.2.4. Types of defects in deep-drawing process

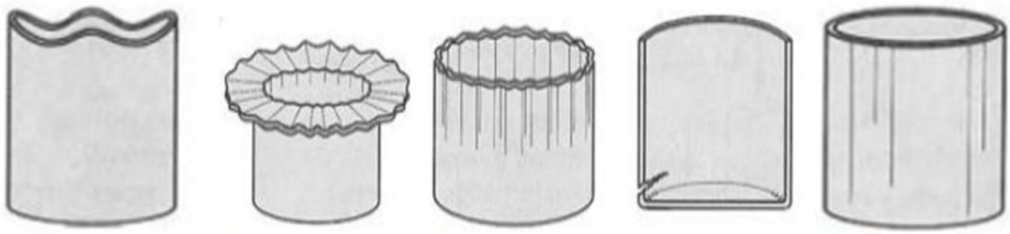

Figure.4: a) Earing b) Wrinkling on flange c) Wrinkling on walls d) Tearing e) Scratches on wall [13]

Earing

Earing is one of the most typical and prominent defects in the deep drawing process. It is the formation of uneven surfaces or waviness on the rim of the sheet metal as seen in Figure.4 a) and Figure.5. It is seen that earing is predominant in anisotropic material and because of planer anisotropy there is a variation of the strength of sheet metal in one direction of a metal sheet to that in another direction[26]. This variation in the strength of sheet metal in a different direction of planes causes an indifferent flow of material and can be marked on the upper rim of the cup in the shape of an ear-lobe like shapes. There can be two, four, and even six ears on the outer surface depending on the plane orientation[27]. The worst one is 8 ears in case of the brass blank. Earing is not at all desirable as it results in the extra trimming of excess material and wastage. Practically we take enough material so that it can be trimmed after trimming.

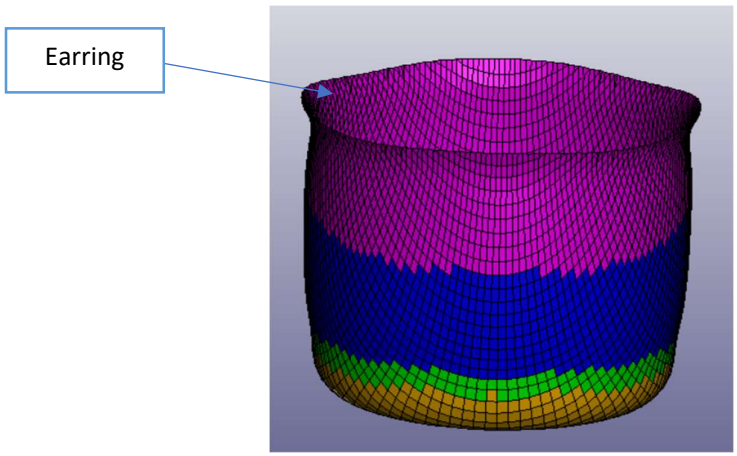

Figure.5: Earing marked on the rim of the cup

Galling

Galling refers to a defect in the die surface in deep drawing operation when during the process there is a transfer of the cup surface particles onto the surface of the die which is in direct contact. This will result in severe damage of die after prolonged usage. It is possible to minimize this defect by opting for a good quality surface and using lubricants. Lubricants reduce friction between parts in contact[14].

Tearing

Tearing is likewise a notable defect in the deep drawing process as seen in Figure.6 which can also be regarded as a limitation till which formability is feasible. Tearing can emerge in the drawn cup if the blank holding pressure is significantly high. The high pressure prevents the sheet metal to slide and bend over the surface die profile. Tearing can be observed near the inner region of the sheet profile at the annular rim[14]. Tearing also occurs near the base of the drawn sheet in the clearance region if the stress value surpasses the strength of the sheet. This will result in severe thinning and finally tearing off the sheet[13].

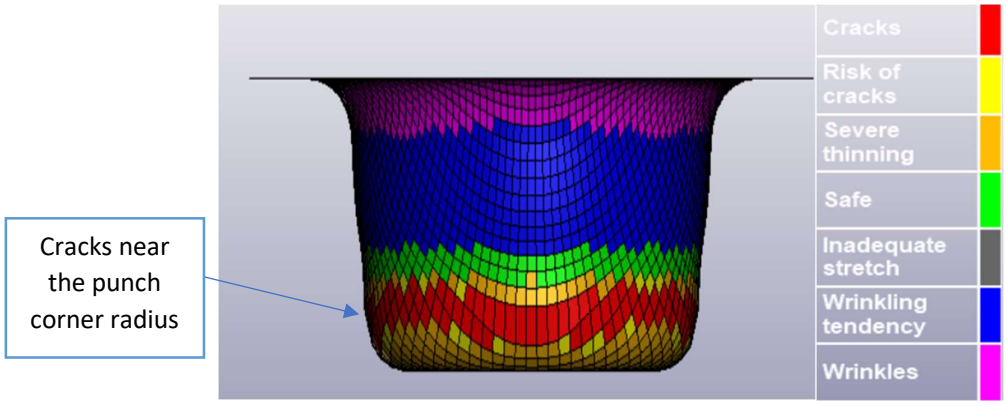

Figure.6: Tearing at the punch corner radius

Wrinkling

The most familiar defect specifically in the deep drawing process is wrinkling visible in Figure.7. Wrinkling arises either on the flange surface of the cup or on the walls of the cups that are being drawn. Considering flange wrinkling, it is caused mainly due to formation of induced compressive stress. There is a series of ridges on the flank surface and it can be avoided by increasing applying blank holding force but up to an appropriate level[14].

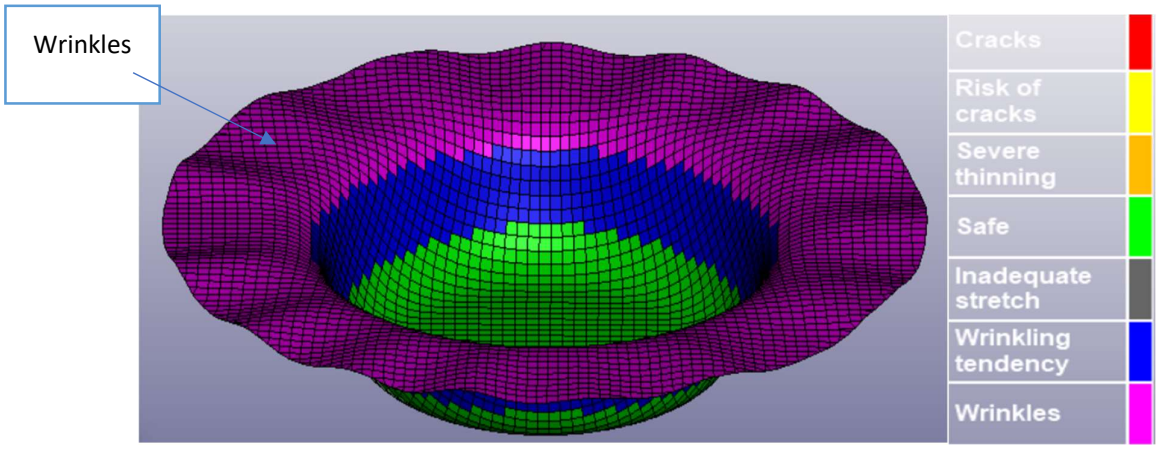

Figure.7: Wrinkling occurring on the flange surface of a drawn cup

If we increase the BHF to a large value it will itself cause necking and eventually failure. Many researchers tried to optimize the blank holder force to avoid wrinkling[28]. When the waviness or ridges on the flange of the sheet is drawn eventually inside, the ridges appear on the wall of the cup[13].

1.2.5. Forming Limit Diagram

The ability of the sheet metal to deform into the required form and size without failure or necking is known as sheet metal formability. We can deform the sheet metal up to a certain limit and that curve that illustrates the limit of formability in sheet metal is called Forming limit curve (FLC). FLC is used to plot the forming limit diagram as shown in Figure.8 [29].

Forming limit diagram is a way of representing the limits of major and minor stress by graphical depiction. It mainly shows where the local necking starts. In a forming operation we know that if the material fails that is there is crack formation, it reaches the limit but here we usually consider local necking as unacceptable. So FLD is very vital in predicting the forming limit and behaviour of sheet metal.

FLD can be mapped by plotting the two mutually perpendicular axes i.e., major and minor strains on a graph paper. The failure criteria can be then plotted on the axes.

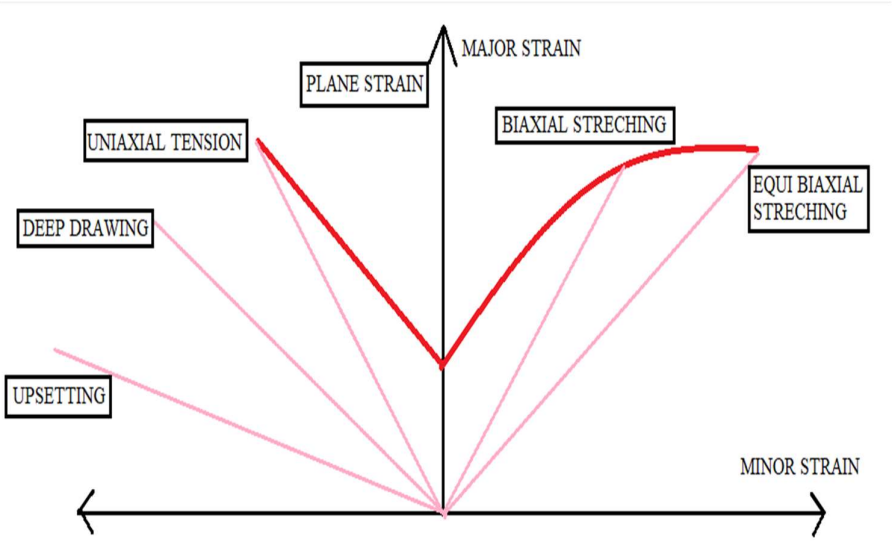

Figure.8: A schematic plot of forming a limit diagram

The FLC curve can be visualized from two sides i.e., the right side and the left side. Keeler and Backhofen [30] scrutinized the right side of the curve and discovered that it is true for positive major strain as well as for positive minor strain. The other side i.e. left side of the FLD curve was presented to us by Goodwin [31] and he uncovered that the left side is valid for positive major strain but negative minor strain. The left branch of the FLC has a strain ratio that can be altered from uniaxial compression (upsetting), uniaxial tension where $\alpha = -0.5$ to plane strain where $\alpha = 0$. On the other hand, the right-side branch has strain ratios that can be ranged from plane strain ($\alpha = 0$) to equibiaxial stretching ($\alpha=1$). As we don't want our model to fail abruptly so we keep a safety limit of 10% which is also known as the safety margin [32]. Any value which will be less than the safety main will not neck and fail. So, if a strain value is close to the FLC of Forming limit diagram it is susceptible to necking and failure.

So experimentally we can find the FLD by the two very renowned methods a) Marciniak tests where the flat-bottomed cylindrical punch is used to strain the sheet metal which is having frictionless in-plane deformation. B) Nakajima tests are used on a sheet metal where the hemispherical punch is used at different sheet widths. To conduct the FLD experiment on a sheet metal we will first draw grids on the sheet. Inside the grid, we will draw circular marks of diameter d_1. On execution of the process, the blank holder will press the sheet and apply pressure. After certain pressure is attained and the sheets gets locked, the punch will start to travel and move towards the sheet. The punch will then deform the sheet to form a dome shape. The circles also get stretched and will result in the shape of an ellipse[32].

Therefore, d_{2minor} and d_{2major} are the final diameters of new formed ellipse. Now$\ln(d_{2major}/d_1)$ and $\ln(d_{2minor}/d_1)$ are the major and minor principle strain. These values are employed to locate the safe region and stay away from necking and failure. The final diameter of the deformed circle i.e., ellipse becomes d_{2minor}(minor diameter of the ellipse and (major dimeter of the ellipse). Principle strains can be found out for the major strain in the direction of the major axis of the ellipse is $\ln(d_{2major}/d_1)$ and the minor strain is $\ln(d_{2minor}/d_1)$. These values at failure and necking give the failure and necking condition, strain values away from the necking gives the safe region [8].

1.3. **ALUMINIUM ALLOYS**

Aluminum comprises of 8% of earth crust and is the most abundant mineral on earth. An aluminum alloy that is basically is a type of has aluminum as a dominant metal in it. The properties offered by aluminum and its alloys make them vital and attractive. These metals and alloys are used not only in kitchen appliances to foils but also in high-end engineering applications like aerospace parts, automobile equipment etc. Aluminum is utilized after steel in structural use. With the growing demand of aluminum as an alternative to steel increases because of its welding capability and enhanced mechanical properties, the study of aluminum and its research is of keen interest. To understand in great dept the properties and characteristics of each family of aluminum alloy we have known the designation and identification of aluminum alloy series[33].

1xxx Series Alloys: This series has 99% aluminium in the alloy and are also named as 'pure aluminium' alloy. They cannot be heat treated and only depend on cold-work and solid solution strengthening to strengthen the properties. These series of alloys can be welded but they have a small range of melting. These alloys have exceptional corrosion resistance; therefore, they are primarily demanded where corrosion is the major criterion in piping and tanks. They have comparatively poor mechanical properties and have applications in structural areas [34], [35].

2xxx Series Alloys: In these aluminium alloy series, copper is added in the range of 0.7-0.8% which improves the strength and performance. The alloys are heat treatable and with varied temperature range, it shows remarkable strength. Few alloys in this series cannot be arc welded as a consequence of hot and stress corrosion cracking. Others can be welded after following the proper procedures [34], [35] .

3xxx Series Alloys: These aluminium alloy series have manganese as an alloying element in the range of 0.05-1.8% which enhances the formability and corrosion resistance but introduces moderate strength. These are non-heat-treatable and work best at high temperatures; therefore it finds application in heat exchangers, power plants, and kitchen appliances like pots and pan. The moderate strength prevents them for usage in structural applications [34], [35].

4xxx Series Alloys: These aluminium alloy series have silicon as alloying additives in the range of 0.6-21.5% which aids in lowering the melting point and enhancing the fluidity. This series has the property that it contains heat treatable as well as non-treatable alloys. They find application as a filler material that can be used in fusion welding as well as brazing [34], [35].

5xxx Series Alloys: These aluminium alloy series have magnesium added as alloying elements in the range of 0.2-6.2% which introduces high strength and they also have comparatively higher strength among non-heat-treatable alloys. These alloys have excellent weldability and for this reason, it is used in various application in the field of aerospace, automobile, construction, etc. If the magnesium content is more than 3%, it is susceptible to hot cracking, therefore it is recommended to use 2.5% magnesium for welding application [34], [35].

6xxx Series Alloys: These aluminium alloy series have magnesium and silicon as alloying elements in an amount of 1%. They have excellent welding properties and are therefore used in fabrication and structural applications. The alloying element forms a solid solution compound of magnesium-silicide that enhances the strength of the aluminium alloy. These are heat treatable and susceptible to solidification crank, therefore not appropriate for arc welding without filler material. Addition of filler material enhances dilution in the arc welding process [34], [35].

7xxx Series Alloys: These aluminium alloys has zinc as an alloying element and are added in the range of 0.8-12.0%. These alloys have highest strength among any other series of alloys. These alloys are heat treatable and find application in the field of aerospace, automobile and high-performance area. The most common alloy from 7 series is 7005 [34], [35].

8xxx Series Alloys: This aluminium alloy has lithium as an alloying element which has a very low density as compared to aluminium. The most common among them is 8011 alloy which is used to make bottle caps. This alloy increases stiffness and respond to age hardening, The application includes aerospace because of low density [34], [35].

1.4. Aluminum alloy temper designation

F — As fabricated – Refers to aluminum alloy temper designation where the alloy is not subjected to temperature treatment or strain hardening

O — Annealed – Refers to heating material for an appropriate amount of time and holding it for certain period. It is then cooled slowly (usually within the furnace) which results in a reduction in hardness and improved ductility. The grains are refined and internal stresses are eliminated on annealing. It is performed to improve machining and plasticity.

H — Strain hardened – Refers to temper designation where cold working is performed on the product to impart strength. It is followed by optional heat treatment which will slightly reduce strength.

W — Solution heat treated – Refers to temper designation applicable to alloys where after heat treatment it ages even at room temperature

T — Thermally treated - Refers to temper designation of any heat treatable alloy which is solution heat-treated followed by quenching and aging.

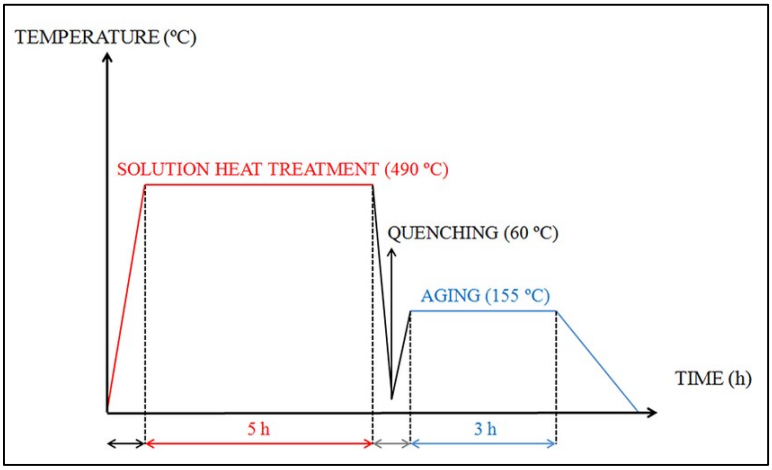

Figure 9: Representation of stages in T6 heat treatment [36]

1.5. Precipitation Hardening

Precipitation hardening is a technique that is carried out by solutioning and quenching. For AlMgSi alloys, precipitation hardening is the most crucial process. We have a second phase which is a solid mixture at a temperature of an elevated state. This solid-phase precipitates as

we quench age. In a ductile matrix, tiny particles are mixed which will aid in improving the mechanical properties. The phase should have solubility in decreasing state with a lowering in temperature and be soluble at increased temperature for precipitation as shown in Figure.10

In AlMgSi-alloys, the primary alloying elements Mg & Si are the second phases of the alloy. Phase diagram show solubility as a function of temperature for Mg and Si as a phase of Mg2Si.In the precipitation process, the alloy is first heated at or beyond solvus temperature for it to produce a homogenous solid solution α. Solving assists to remove dislocations and grain structures from the solution. Therefore, it helps in the dissolution of the phase.

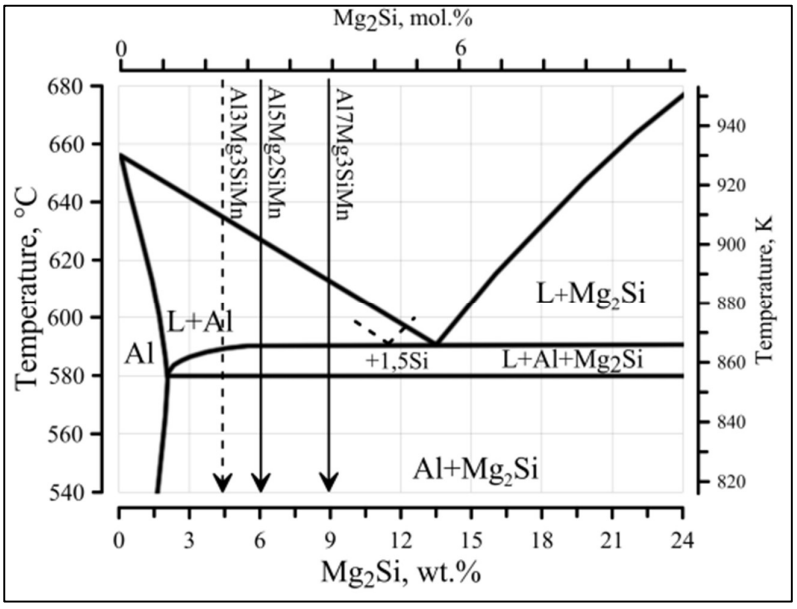

Figure 10: Al-Mg2Si Phase diagram [37]

Quenching by water or air is done when we reach solubilization temperature. It forms an unstable supersaturated solid solution at the nucleation sites. For this reason, we have a decline in solubility with a falling temperature. When the temperature was raised to near 160-200 °C we have a supersaturated alloy that will get ageing artificially.

1.6. Annealing

During the metalworking process, the grains are cold worked and stretched and their dislocation makes them stronger and brittle or we can say somewhat less ductile. In the metal forming process, we need soft material of good ductility. So, to achieve a soft material we heat

the material inside the furnace. There are phases during the heating *-+phase (a) recovery (b) recrystallization and (c) grain growth.

Annealing is a heat treatment process to soften the material. In a cold-worked process, the internal energy is always higher because of the absorbed energy as a result of the plastic deformation. Therefore, we will have high internal energy in a cold-worked than in an unworked process.

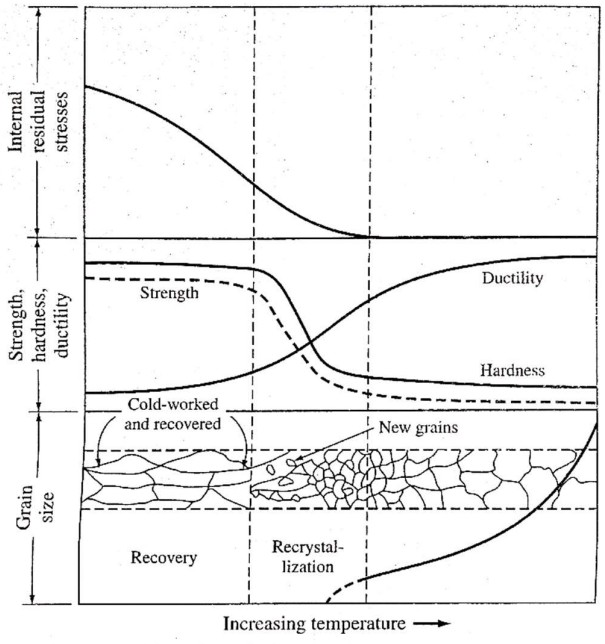

Figure.11: Shows the effect of temperature on the mechanical properties of the materials. [38]

When we heat the material above the recrystallization temperature, the internal stress gets relieved. The dislocation takes energy to rearrange itself to attain a lower energy state. The polygonization process occurs where sub-grain boundaries occur due to the recovery phase. As the dislocation arranges itself into a lower energy state after their movements are stopped, therefore we have lower internal energy. This will lead to an increase in ductility but somewhat reduction in strength

We know that in recrystallization of the cold-worked material, new grains replace the old grains. The nucleus grows and the high-angle grain boundary becomes highly deformed. In the annealing, process material is heated at a high temperature. We then have a soaking temperature. Eventually, we cool it to room temperature. Time is the key factor.

1.7. LS-Dyna FEA Software

LS-DYNA is well known multi-physics software that is used for advanced simulation. It was developed by Livermore Software Technology Corporation (LSTC). It was afterward acquired by Ansys software company in the year 2019. LS-DYNA is used to solve real-life problems like the crash test, explosions, forming, and much more. This software is used by every field of engineering like software, mechanical, aerospace, design, civil, military, and bioengineers.

The beginning of fast, large memory capacity, graphically enhanced computers in the early 1990s helped in visualization (simulation) of sheet metal forming operations like stamping, deep-drawing, forging, hydroforming, and many more. There is a large amount of data analysis required in actual testing so this becomes comparatively easy as choosing the required output in simulations is quite easier. Thus, the simulation analyzed through non-linear finite element analysis has become an important tool in optimizing and examining metal forming operations.

Moreover, in LS-DYNA FE simulations other than sheet metal forming can also be observed. The advanced technology which improved the visualization also permitted to have a better understanding of vehicle crashes by fast analysis through videos of a car crashes in actual scenarios. The static problems can also be solved in this software. The acceleration, forces, displacement, velocity, stresses, and strain can also be calculated for dynamic problems for vehicles and normal parts.

1.8. Yield Criteria

The yield criteria of any material define the limit for the start of the plastic region or we can say the end of the elastic behaviour. When the material reaches the yield stress in a uniaxial compression or tensile test, it commences to flow plastically[8] .

$$\sigma = \frac{P}{A} = \sigma_y \tag{6}$$

Where,

P	Instantaneous force
A	Instantaneous area of the test specimen
σ_y	Yield stress of a material in tensile test
σ	Stress experienced by a material

The most popular yield criteria which are widely used for isotropic and anisotropic material are listed below:

Isotropic yield criteria

- Tresca /shear stress yield criterion
- Von Mises / distortion energy criterion

Anisotropic yield criteria

- Hill's 1948 yield criterion
- Hill's 1990 yield criterion
- Barlat 1996 yield criterion

Initially, without the proper knowledge of anisotropic material and the state of stresses, isotropic yield criteria were used everywhere. It was very convenient for us to do conduct a uniaxial tensile test and find the yield stress using Tresca and von-mises yield criteria. After a deep study in the field of anisotropic material, it was found that anisotropic material doesn't give accurate results with the above yield criteria. Therefore, in 1947 Hill's introduced the world with Hill's 1948 yield criterion and opened endless research in the field of anisotropic yield criteria.

The rolling of the sheet metal is the main reason for the anisotropic characteristics. The rolling process aligns the grains along the rolling direction and therefore we have different properties in rolling, transverse as well as in thickness directions. So to work on anisotropic material various yield criteria are used and the most popular among them are the Hill's and Barlat criteria. There is constant modification still happening in this regard which lead to different yield criterions in different years of research[8].

1.8.1. Hill's 1948 yield criteria

Hill's criteria are the most popular and widely used yield criteria because of its simple behaviour. This criterion has less number of parameters with simple, easy to relate, and

physically defined parameters. The assumptions used in this criterion are easy to understand [3].

$$2f(\sigma_{ij}) = H(\sigma_x - \sigma_y)^2 + G(\sigma_z - \sigma_x)^2 + F(\sigma_y - \sigma_z)^2 + 2N\tau_{xy}^2 + 2M\tau_{zy}^2 + 2L\tau_{xz}^2 = 1 \quad (7)$$

Where,

σ_x , σ_y , σ_z , σ_1 , σ_2 , σ_3	Normal stress in x, y, z direction
τ_{xy},τ_{zy}, τ_{xz}	Shear stress
F, H, G, N, L, M	Anisotropic constants of the yield criterion

Hills criterion in terms of constants is given as

$$\bar{\sigma}_0^2 = \frac{r_0 r_{90}(\sigma_y - \sigma_x)^2 + r_{90}\sigma_x^2 + r_0\sigma_y^2 + (2r_{45}+1)(r_0 + r_{90})\tau_{xy}^2}{r_{90}(r_0+1)} \quad (8)$$

When stresses in orthotropic axis are replaced by stresses in principle directions ($\sigma_x = \sigma_1$, $\sigma_y = \sigma_2$, $\tau_{xy} = 0$) the Eq. (8) changes to Eq. (9)

$$\bar{\sigma}_0^2 = \frac{r_0 r_{90}(\sigma_1 - \sigma_2)^2 + r_{90}\sigma_1^2 + r_0\sigma_2^2}{r_{90}(r_0+1)} \quad (9)$$

Where, $\bar{\sigma}_0$ is the flow stress in uniaxial stress and is given by the:.

$$\sigma_1 = \frac{F}{A} = \bar{\sigma}_0$$

This yield criterion only require plastic strain ratio in the rolling, diagonal, and transverse directions as r_0 , $r_{45}$and r_{90} and hence most preferred and widely used. But Hills criterion also has some drawbacks which is also regarded as anomalous behaviour,

a) First order anomalous Behaviour

In case of equal biaxial stress,

$$\sigma_1 = \sigma_2 = \sigma_b$$

Where σ_b is the biaxial stress, and σ_1 and σ_2 is the stress in two principle direction.

The Hill's yield criteria in the Eq. (8) gets reduce to give results as,

$$\sigma_b = \bar{\sigma}_0\sqrt{\frac{1+r}{2}} \quad \text{or} \quad \frac{\sigma_b}{\bar{\sigma}_0} = \sqrt{\frac{1+r}{2}} \quad (10)$$

If r >1 then $\sigma_b > \bar{\sigma}_0$ and if r < 1 then $\sigma_b < \bar{\sigma}_0$

The biaxial stress is proportional to the plastic strain ratio 'r' from the Eq. (10). We know that the r value of aluminium is less than 1 but the results we found were totally opposite. The yield value of biaxial was greater than instead of lesser than the yield value of tensile test [3] [8].

b) Second order anomalous Behaviour

If we consider deformation along transverse direction for a tensile test before necking or bulging ($\sigma_y = 0$ or $\tau_{xy} = 0$), the yield along transverse direction can be shown according to Eq. (11)

$$\sigma_y = \frac{\mathrm{F}}{\mathrm{A}} = \overline{\sigma}_{90} \tag{11}$$

Where, $\overline{\sigma}_{90}$ is flow stress along transverse direction in uniaxial tensile test.

The The Hill's yield criteria in the Eq. (8) gets reduce to give results as,

$$\bar{\sigma}_0^2 = \frac{r_0(r_{90}+1)\bar{\sigma}_{90}}{r_{90}(r_0+1)} \text{ or } \frac{\bar{\sigma}_0}{\bar{\sigma}_{90}} = \sqrt{\frac{r_0(r_{90}+1)}{r_{90}(r_0+1)}} \tag{12}$$

This equation represents that if $\frac{r_0}{r_{90}} > 1$, then we will have $\frac{\bar{\sigma}_0}{\bar{\sigma}_{90}} < 1$ and vica-versa. But, there are many alloys which do not follow this behaviour and hence Hill's criterion cannot be used everywhere [3].

Also, the hill's criteria are only applicable to deep drawing process having only 4 ears. But there can be a possibility of more than four ears. Therefore, we have to choose some other yield criteria. Hence, we prefer to use Barlat for aluminium.

1.8.2. Hill 1979 Yield Criterion

As the 1948 quadratic model was not suitable for aluminium alloys, Hill's proposed another model which is based on non-quadratic criteria and is given by Eq. (13).

$$f\,|\sigma_2 - \sigma_3|\,m + g\,|\sigma_3 - \sigma_1|\,m + h\,|\sigma_1 - \sigma_2|\,m + a\,|2\sigma_1 - \sigma_2 - \sigma_3|\,m + \\ +b\,|2\sigma_2 - \sigma_1 - \sigma_3|\,m + c\,|\sigma_3 - \sigma_1 - \sigma_2|\,m = \sigma_m \tag{13}$$

This model still cannot predict the behaviour of the materials having

$$\frac{r_0}{r_{90}} \neq 1 \frac{\sigma_0}{\sigma_{90}} \neq 1 \tag{14}$$

and as the value of m is a non-integer, we have to perform numerical analysis for even simple cases.

There is more improvement by hills in its model in 1990 and 1993 which is very complex to find parameters and even does not contain crystallographic structures in consideration. Therefore, there were modification on Hill's model by Hosford and barlat [3].

1.8.3. Hosford Yield Criterion

Hosford proposed an independent yield criterion, different from Hill's given by Eq. (15)

$$F\,|\sigma_{22} - \sigma_{33}|^{m} + G\,|\sigma_{33} - \sigma_{11}|^{m} + H\,|\sigma_{11} - \sigma_{22}|^{m} = \sigma_m \quad (15)$$

The main difference between hills and Hosford was the Hosford also took into consideration the crystallographic structure of the material and related it to the value of m. He considered m=6 for BCC material and m=8 for FCC material.

If we plane stress, the equation then reduces to,

$$r_{90}|\sigma_{11}|^{a} + r_0\,|\sigma_{22}|^{a} + r_0 r_{90}\,|\sigma_{11} - \sigma_{22}|^{a} = r_{90}(r_0 + 1)\,\sigma_0^{a} \quad (16)$$

1.8.4. Barlat 1989 Yield Criterion

Logan and Hosford proposed [39] a yield criteria which is based on the principle deviatoric stresses and they equated with the mean stress which was considered to independent of mean stress[3].

$$\emptyset = |K_1 - K_3|^{m} + |K_2 - K_3|^{m} + |K_2 - K_1|^{m} = 2{\sigma_Y}^{m} \quad (17)$$

This Eq. (17) is a generalized form, it will reduce it to Von-mises if the value of m=2 and when the value of m=1 or ∞ it will reduce itself into Tresca yield criteria [8].

Barlat and Lian [40] then introduced parameters such as a, c, h, p to the Hosford Eq. (17) for plane stress condition.

$$\emptyset = a|K_1 + K_2|^{m} + a|K_1 - K_2|^{m} + c|2K_2|^{m} = 2{\sigma_Y}^{m} \quad (18)$$

Where, K_1, K_2 are given by the Eq. (19) and Eq. (20) respectively

$$K_1 = \frac{\sigma_x + h\sigma_y}{2} \tag{19}$$

$$K_2 = \sqrt{\left(\frac{\sigma_x - h\sigma_y}{2}\right)^2 + p^2\tau_{xy}^2} \tag{20}$$

The parameters such a,c,h can be found out by considering plastic strain ratio as shown in Eq. (21) – (23)

$$a = 2 - 2\sqrt{\frac{R_{00}}{1+R_{00}} \cdot \frac{R_{90}}{1+R_{90}}} \tag{21}$$

$$c = 2 - a \tag{22}$$

$$h = \sqrt{\frac{R_{00}}{1+R_{00}} \cdot \frac{1+R_{90}}{R_{90}}} \tag{23}$$

According to 'Barlat and Lian' the *R*-value, width to thickness strain ratio, for any angle ϕ The following Eq. (24) can calculate the value of p iteratively [41]:

$$R_{\emptyset} = \frac{2m\sigma_Y^m}{\left(\frac{\partial \emptyset}{\partial \sigma_x} + \frac{\partial \emptyset}{\partial \sigma_y}\right)\sigma_{\emptyset}} - 1 \tag{24}$$

The yield strength of the material can be expressed in terms of k and n given by Eq. (25):

$$\sigma_y = k\varepsilon^n = k\left(\varepsilon_{yp} + \bar{\varepsilon}^p\right)^n \tag{25}$$

Where,

m	Non-linear relationship coefficient
a, c, h, p, m	Anisotropic material parameters
σ_y	Yield stress of material
K_1,K_2 , K_3	Principle deviatoric Stress

The Barlat has only 4 parameters to be identified therefore it is slightly easy to find (except p parameter). Without having high anisotropy it gives very good yield locus of aluminum [8].

1.9. Stress and Strain Calculations

If we consider a dogbone shape specimen that will be strained on a UTM machine. The force 'F' that is applied to the specimen will be uniaxial in the tensile direction. The area of the specimen will be calculated in a cross-sectional plane referred to as A_o. The original gauge length will be measured before testing and denoted as L_o [8].

The enginnering stress σ_e was estimated from the Eq. (26) which formulates that enginnering stress will be equal to the average of the perpendicular force 'F ' divided by the original area of cross-section 'A_o'. The SI unit for stress is newton per meter square (N/mm^2) which is similar to the unit of pressure so we can also use Pascals (Pa). As the force which is applied on the specimen is in the perpendicular direction, the enginnering stress σ_e is also commanly reffered to as the nominal stress [16][8].

$$\sigma_e = \frac{F}{A_o} \tag{26}$$

Now on UTM machine when we will elongate the specimen in the uniaxial tensile direction, the length of the specimen will change. The cross-sectional area will reduce and the consecutively length will increase. The original length of the specimen was L_o then the final length of the specimen after elongation and removal of load will be L_1. The change in the length that is '$L_1 - L_o$' will be calculated as ΔL [8].

The enginnering strain will be calculated from the Eq.(27) and can be formulated as the change in length of the specimen divided by the original length before conducting the tensile test. As enginnering strain is the ratio of length, the SI unit be unitless [8].

$$\varepsilon_e = \frac{\Delta L}{L_o} \tag{27}$$

In various cases of compression and extension where the plastic strain was high, it was discovered that engineering strain was not able to predict the deformation accurately. The cases of compression and extension were not symmetric and in even more complicated situations the results were appropriate. To overcome this anomaly, engineering strain was converted to true strain[8]. The engineering strain will be written in terms of differential equation as shown in Eq. (28) [8].

$$d\varepsilon = \frac{dl}{l_o} \tag{28}$$

After integrating Eq. (28) the over the entire stretching length we will get as shown in the Eq. (29)

$$\varepsilon_t = \int_0^{\varepsilon} d\varepsilon = \int_0^{l_1} \frac{dl}{l} = \ln \frac{l_1}{l_0}$$

$$\varepsilon_t = \ln \frac{l_1}{l_0} = \ln \frac{l_0 + \Delta l}{l_0} = \ln \left(1 + \frac{\Delta l}{l_0}\right) \quad (29)$$

The value of true stress σ_t and true strain ε_t can be calculated from the expression as stated in Eq. (30) and Eq. (31)

$$\varepsilon_t = ln(1 + \varepsilon_e) \quad (30)$$

$$\sigma_t = \sigma_e(1 + \varepsilon_e) \quad (31)$$

1.10. Holloman's equation

The expression in Eq. (32) between true stress and true strain which is used to find strain hardening exponent and strength coefficient. This equation is primarily used in plastic region in metal forming operation [16].

$$\sigma = K\varepsilon^n \quad (32)$$

Where,

n	Strain hardening exponent
K	Strength coefficient

The value of n of metals varies from 0 to 1 where 0 implies that material is perfectly plastic and 1 implies perfectly elastic. The common value of n is between 0.10 - 0.50.

1.11. Volume Constancy during plastic deformation

In plastic deformation, the volume of the metal is constant that is it does not vary as it requires the structure lattice to change. But the deformation in plastic deformation occurs by

slip or twinning which do not change the crystal structure and deformation arises microscopically [8].

So volume before deformation V_0 is equal to volume after deformation V_1 as shown in Eq. (33)

$$V_0 = V_1 \tag{33}$$

This can be also re-written according to dimensions as

$$a_0 . b_0 . c_0 = a_1 . b_1 . c_1 \tag{34}$$

Eq. (34) can arranged to and then by applying ln on both sides

$$1 = \frac{a_1}{a_0} . \frac{b_1}{b_0} . \frac{c_1}{c_0}$$

$$0 = \ln\frac{a_1}{a_0} . \ln\frac{b_1}{b_0} . \ln\frac{c_1}{c_0} \tag{35}$$

From the Eq. (35) we describe the equation the Eq. (36) as a sum of three strains in three directions as:

$$\varepsilon_a + \varepsilon_b + \varepsilon_c = 0 \tag{36}$$

1.12. Johnson–cook flow stress model

Johnson–cook is empirical based constitutive model that was proposed by Gordon R. Johnson and William H. Cook [42]. The main purpose of this model is to save computational time in the process of high velocity impact, explosion and detonation [43]. The model is basically used to visualise the cumulative effect of strain hardening, strain rate and softening under thermal effects on a material. It is a very basic model with a smaller number of parameters to be estimated [44]. Therefore, many researchers deploy this model in their research to find the equivalent flow stress under the action high strain, strain rate and temperature.

J-C model equation can be formulated as shown in Eq. (27):

$$\sigma_e = \left(a + b\varepsilon_p^n\right)\left(1 + cln\frac{\dot{\varepsilon}}{\dot{\varepsilon_o}}\right)(1 - T^{*m}) \tag{37}$$

Where,

$$\dot{\varepsilon}^* = \frac{\dot{\varepsilon}}{\dot{\varepsilon_{ref}}}$$

$$T^* = \frac{T - T_{ref}}{T_m - T_{ref}}$$

CHAPTER 2
LITERATURE REVIEW

2.1. LITERATURE REVIEW

A C Sekhara Reddy et al. [45] presented a unique technique of LDR on the fracture for rapid development at characteristic limit load. This method requires only three sizes of samples hence reliable and consuming less time. Aluminum alloy sheet AA6111 is used to carry out experiments that are widely used in automobiles. LDR was found to be 2.37 which aligned with the others researched pieces of literature.

Farhang Pourboghrat et al.[46] conducted forming experiments of AA5754 aluminum sheets. Punch was cylindrical at varying temperatures and pressures. The LDR was at calculated 1.33 for sharp radii and 2.21 round die corner radii. Temperature-dependent FLD was used to predict the commencement of wrinkling and tearing.

Bharath Patil et al.[47] studied the factors which affect the deep-drawing process. Punch velocity and die corner radius is varied from 850mm-s till 950mm-s and 2mm till 7mm respectively. Blank holding force and co-efficient of friction were constant. Solid Edge V19 was used for CAD modeling and AFDEX software for simulation. Aluminum Alloy AA6061 material was used at room temperature. It was found that punch velocity increased damage value and the increase in die corner radius decreased damage value. At the last optimized parameters was calculated.

M.T. Browne et al.[48] explored the variation and consequences of numerous factors in deep-drawing. In the experiment C.R.1 cups were taken with a thickness of 0.9 mm. An L8 orthogonal array screening experiment was conducted after drawing a series of cups. The factors were varied at various levels. The punch load and wall thickness were picked responses. The experimental work was carried out to optimize these factors. The lubricating die side gave more acceptable results than the punch side. TRP of 70 KN, BHP of 18 KN, and speed of 100 mm/min were optimal parameters providing the least variation.

Dr. R. Sridhar et al.[49] presented micro deep-drawing process for use in producing cups, boxes instead of other micromachining methods. He talked about the problems of wrinkling in the deep-drawing process and the parameters such as coefficient of friction, blank holding force, die radius, etc. which are to be selected carefully for minimum defects. It was concluded that thicker material has larger LDR having the identical punch.

Swadesh Kumar Singh et al.[50] examined the deep drawing process of forming at elevated temperatures. The LDR and coefficient of friction were calculated for steel at 25° C temperature and 200° C. It was inferred that there is an rise in LDR with an escalation in temperature because of relief in stress for both simulations in Ls-Dyna and experimental work. There was a consistent distribution of thickness in drawing at raised temperatures.

Liwen Tian et al.[51] researched about thinning in the deep-drawing process using Ls-Dyna software and the orthogonal experiment method. It was deduced that the blank holder force is the most vital factor influencing thickness and another one is the concave die entrance radius. The Punch velocity and the radius had bare minimal impact.

Tahir Altinbalik et al.[52] studied the variation in steel sheet thickness with the help of simulations and confirmed the outcomes in experimental work in the deep drawing process. FLD was generated by conducting forming limit test. Then various blank holding forces were applied by gas springs. Simulations were performed in AUTOFORM software. There was a consensus between calculated and simulated results.

Amr Shaaban et al.[53] researched on the die-geometry, cushioning, and punch movement in the deep-drawing process. The diverse parameters were investigated for a deep-drawing process without a blankholder but with added cushioning. Ls-Dyna simulations were accomplished to analyze the effect of these parameters on load and thinning. It was inferred that cushioning and thickness have a significant effect and punch speed shows minimal effect.

Devendar.G et al.[54] investigated parameters such as coefficient of friction, punch velocity, blankholding force, temperature, and thickness in a deep-drawing to minimize defects. It was seen that the blank thickness has a significant impact on stress. An upsurge in temperature softens the material and therefore stress gets relieved. The normal-pressure increases between the die and blank because of a rise in stress as the coefficient of friction increases. The blank holding force regulates the wrinkling effect and thickness variation. It was also inferred that by carefully optimizing the blank shape we can control tearing, and wrinkling and can also minimize the forming load.

G. Behrens et al.[21] investigated the various parameters impacting the limiting draw ratio in micro-deep drawing, at different die radius, punch diameter and die clearance, test was conducted to find limiting drawing ratios. Al99.5 and E- Cu58 with 20 mm thickness each 25mm thickness X5CrNi18-10) were examined. There is an increase in LDR with an increase in die radius for E- Cu58 and steel.

Jay N. Mistri et al.[55] investigated reduction in wrinkling, tearing, and fracture defect by various process parameters like punch velocity, punch force, sheet thickness, and blank force in forming process. Experimental as well as simulation results were used to calculate stress-strain distribution. It was concluded that lubrication can reduce wrinkling and other results were in agreement.

Di Pan et al.[56] investigated micro deep drawing at various velocities. Three different thickness of stainless steel was annealed under argon gas. These sheets were drawn at different velocities. At thin sheets, earing becomes prevailing and wrinkling slowly vanishes. Sheet surface becomes smooth with thickness and drawing velocity.

Gyadari Ramesh et al[57] studied blank holding force as it is the major parameter to arrest wrinkling and tearing. 30mm diameter is taken for 1 mm thickness and simulations are conducted in Ls-Dyna. An increase in BHF increases frictional force, therefore tensile stresses guide to tearing failure at the punch corner. There is an optimum BHF where no wrinkles are formed and also stresses are minimum.

M. Jain et al.[58] scrutinized the rapid development of LDR of AA5754-O and AA6111-T4. The parameters such as punch load vs displacement, flange draw-in, strain distribution on the wall of the cup, wrinkling, ironing, and fracture were analyzed. A decline in the value of LDR and flange draw-in was observed with the die profile radius. Both the materials displayed equivalent depths of the draw, and punch displacement values for maximum punch load. The limiting draw ratios (LDRs) for AA5754-O are higher than AA6111-T4. The LDR reduces with a reduction in the die profile radius. AA6111-T4 was more sensitive to this outcome than AA5754-O due to its moderately lower n value and lower bendability.

G. Ganesh Niranjan et al.[59] investigated the formability of aluminum alloys for automotive applications. As the plastic strain ratio of aluminum is poor than steel, a study was conducted on three different rolling directions. Swift cup forming at 0 and 45 enhanced LDR to 2.1 from 1.96.

You-gen WANG et al.[60] conducted a deep-drawing experiment to inspect the significance of the blank holder on drawability and defects. A flat and curved blank holder was used for this pursuit. The flat blank holder possesses an LDR of 1.7 with a severe earring. With the introduction of a curved blank holder, LDR was improved to 2, and earing was also minimized.

Eric T. Harpell et al.[61] predicted the LDR of a cup-drawing for AA5754-O by drawing 10 different geometric tools in Ls-Dyna explicit solver. Various yield criteria were used and prediction of punch velocity, punch force, and stress-strain distribution was achieved. The Barlat-89 yield criteria were more precise than von-mises as well as hill's criteria. For punch profile radius greater than 3mm the model was showing an accurate result.

Nitin Kotkunde et al.[62] commented that proper simulation models are only attainable when we decide and implement correct material model cards and input parameters. He has taken Ti–6Al–4V alloy for the study of different yield criteria like 'Hill 1948', 'Barlat 1989', 'Barlat 1996', 'Barlat 2000' and 'CazacuBarlat' at 400° C. These yield criteria were utilized in the simulation research of the deep drawing process. An experimental deep-drawing process was also conducted to demonstrate the results. CazacuBarlat was found to be more satisfactory anisotropic yield criteria which were confirmed with the experimental results.

Rubén Lostado-Lorza et al.[63] presented a cup drawing simulation on planer anisotropy using Barlat yield criteria. It was also remarked that barlat is the most convincing yield criteria for aluminum. In the end, it was concluded that maximum von mises was found to be at a location farthest from punch while minimum von mises at the central location, the forming limit was found to be 0.624, and FEM was proved to be advantageous in cold working for non-linear profiles.

Y. Marumo et al.[64] researched on the effect of sheet thickness on blank holding for as well as limiting draw ratio. He found that as we decrease the sheet thickness there is an increase in blankholding force required to remove wrinkling. As we decrease the sheet thickness, LDR also decreases and below 0.04 mm, sheet thickness decreased rapidly.

Hong Seok Kim et al.[65] researched about warm forming and the various factors like temperature, friction, BHF, and punch speed affecting the process. He developed a material mode for analysis with different BH and friction and conducted analysis at different temperatures as well as strain rate. LDR calculation has only 3% deviation from experimental results because of contacts assumptions. To increase the formability, we require lower friction as well as lower BHP since the force resisting the formability will decrease. There is increase

in level of formability at room temperature as LDR values are not affected by forming temperature.

B.V.S.Rao et al.[28] in his research tried to optimize blank holding force using numerical simulation. Different parameters like Die radius, Punch radius, friction and punch diameter was considered. Finite element analysis was performed in hyper mesh and L-27 Taguchi analysis was conducted to determine the effects of process parameters. He was successful in finding the optimum BHF and concluded that punch diameter was the most influential parameter. It was then followed by radius of die, radius of punch, clearance and friction. He found that wrinkling is minimum at 7mm die radius, 1mm of punch radius, 7% of clearance and 0.45 of coefficient of friction

Ravikant Patel et al.[26] conducted finite element modelling to precent earing defects. Mild steel of 1mm thickness and different blank size was considered. Hyper mesh 12 was taken as FEA tool and solver was selected as RADIOSS. Different blank size was considered as it was found that there is a decrease in % height and load. Therefore for a non-circular blank there is less earing defect, and load as in circular blank there is normal anisotropy.

Jigar Pathak et al.[17] studied the state of stress and thickness on the different regions in the cup of deep drawing process. The simulation which was used was PAM STAMP 2G and it was successful in deep drawing the model and checking the state of stress at different dept. The material that was used was Al6061 with sheet of thickness 1mm. At 3 different location stress and strain was analysed to find out the thickness. He concluded that the flange portion gets thickened and the wall portion gets stretched. The bottom region of the cup experiences no change in thickness change.

Devesh Rajput et al. [66] examined stress-strain readings of AA6063-T6 under quasi-static strain at room temperature. These results obtained were employed to find dynamic stress and material constants of the Johnson-Cook model. The numerical results were very near the experimental results.

Sangeeta Khare et al. [67] incorporated the Johnson-Cook material model to anticipate the behavior of armor steel plates at high strain rate (10^{-4}–1550 s^{-1}) and temperature (25–600 °C). At a notch radius and strain rate of 2-20 mm 10^{-3} s^{-1} respectively, the stress and damage models were validated at room temperature which shows good agreement for smaller than larger radii.

Suyang Li et al. [68] predicted the behavior of materials in machining operations. Johnson-Cook model at high temperature(400°C) and strain rate (10^{-4} s^{-}) found by split Hopkinson pressure bar is used to explore the dynamic behavior of AA6061-T6. Cutting force, critical speed, and stress-strain relationship are in consensus with the experimental data.

Wang et al [69]investigated the hot forming process on sheet metal for AA7075-H18 alloy and characterized the material behavior for flow stress accurately by employing the improved Johnson-Cook model. In the hot processing maps, it was concluded that when the temperature was more than 350°C safety region was reached and defects were averted.

R. Seddik et al [70] induced shock waves in a thin foil by laser irradiation to specify yield stress and strain hardening for various metals at a very high strain rate. Johnson-Cook models with and without strain hardening were utilized for simulation in which material parameters were found by comparing the velocity profiles of simulated and experimental results.

Mingzhong Hao et al [71] formulated a machine learning algorithm and swarm optimization techniques to calculate the Johnson-Cook parameters in a porous structure. To simplify the process of finding material parameters, S. Deb et al [72] also developed an artificial neural network model for predicting the flow stress as output similar to the traditional J-C model. It was seen that the ANN technique was more convenient and efficient than conventional techniques.

P. Patil et al. [21] carried out a gas detonation process to form DC04 steel cups and applied the Johnson-Cook material model. He was successful in predicting the damage initiation and evaluation which was close to experimental results.

2.2. Research Gap

A lot of research has been already done on AA6082 alloy but only a few have studied its drawability in the deep drawing process.

As AA6082-T6 is having high strength, only some researchers have annealed the material to attain higher ductility.

Most of the authors have researched drawability without even considering the appropriate material characteristics.

Limited number ofa researcher have considered the combined effect of strain, strain rate, and as well as temperature in the deep drawing operation which is essential to predict the behaviour of the material as close to the real scenario.

Only few parameters affecting drawability are discussed by authors in various research papers.

2.3. Objectives

- To attain higher elongation of AA6082-T6 material by annealing
- To study appropriate material characterization and predict the accurate material behaviour during deep drawing as close to actual experimentation
- To study the Barlat 3 parameter anisotropic yield criterion and calculate its material parameters and constants using tensile and anisotropic tests respectively
- To find material constants for the Johnson-Cook equation for various strain rate and temperatures
- To simulate the deep drawing process is modelled in Ls-Dyna PrePost(R) V4.6.17 software
- To study the various parameters influencing the drawability of AA6082 during deep drawing

CHAPTER 3
METHODOLOGY

3.1. Material Selection

The aluminium 6000 family series has magnesium and silicon as their primary alloying element. These alloying element enhances the properties of 6000 alloy and increases their strength, corrosion resistance, weldability and extrudability. These alloys are having good welding properties and after heat treatment the properties such strength is also increased. Because of the above stated reasons, automobile industries have a particular interest in 6000 alloys. As weight is a important parameter in vehicles, use of aluminium (2700 kg/m^3) is a perfect choice as it one-third the weight of steel (7600 kg/m^3)[33].

We are using AA6082 for our research work as it is having highest strength than other 6000 alloys and 15-20% higher than AA6061 alloy. This high strength is contributed by the addition of manganese which alters the grain structure of 6082 alloy and makes them stronger. This alloy has exceptional corrosion resistance because of lower copper content as compared to AA6061. This alloys also has great ductility, low weight, easy to machine and are popularly known as structural alloys as it is used for transportation and structural application [34][73].

AA6082 has different types of tempers [74] such as

O	Annealed wrought alloy
T4	Solution heat treated & naturally aged
T6	Solution heat treated & artificially aged
T651	Solution heat treated, stress relieved by stretching and then artificially aged

Table. 1: AA6082 alloy chemical composition

Alloy	Mg	Si	Mn	Cu	Cr	Zn	Ti	Fe	Al
AA6082	0.6-1.20	0.70-1.30	0.40-1.00	0.10	0.25	0.20	0.10	0.50	Remainder

3.2. Tensile Test

The uniaxial tensile testing was performed according to ASTM-E8M standard. The specimen was designed as per ASTM standard CAD is shown in Figure.12 and HS-G3015C laser cutting machine was used to machine the tensile specimen. The AA6082 alloy specimens were prepared which has a gauge length of 32 mm. The S-Series of H50KS Bench-top uniaxial tensile testing machine as seen in Figure.13 a) which had a maximum capacity of 50 KN was used to perform the tests and the crosshead speed was given as 2.5mm/min. H50KS Bench-top uniaxial tensile testing machine runs at operating temperature of 0°C-38°C in a 10-90% relative humidity. The input voltage is as per the customer requirement and the power is 500W at 220/240 V with a single phase. To measure the force in the machine uses full bridge strain gauge which has a Z-beam that can be used in tension and compression. It has a resolution of 1/320000 and accuracy of $\pm 0.5\%$. The specimen after failure in the uniaxial tensile machine is clearly seen in Figure.13 b). So the specimen before and after the tensile test in visible in Figure.14.

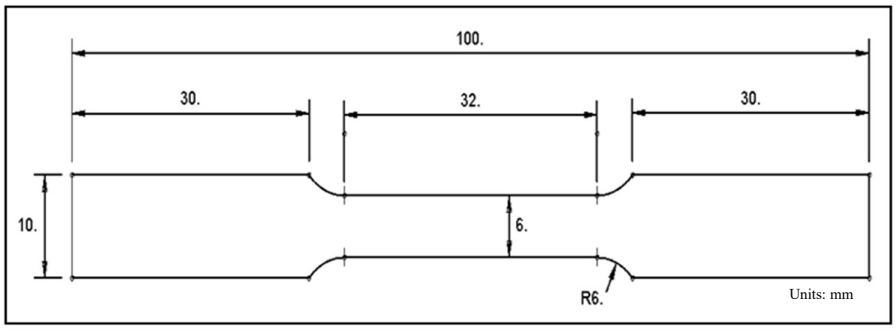

Figure.12: Tensile testing specimen as per ASTM-E8M standard

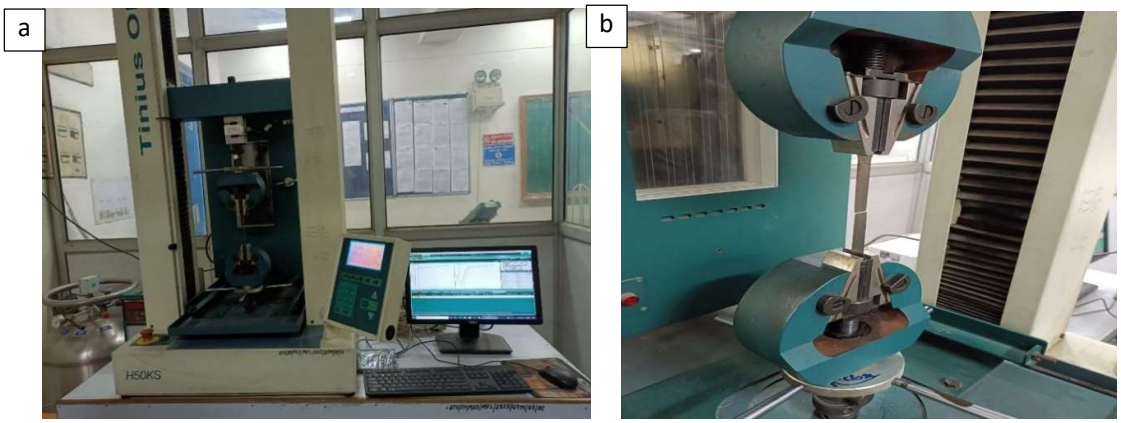

Figure.13: a) Universal Tensile testing machine and the crossheads b) Specimen after failure in Universal Tensile testing machine

Figure.14: Specimen before and after the tensile test

3.3. Determination of True Stress and True Strain Calculations

σ_e and ε_e were calculated from the Eq. (26) and Eq. (27) were other parameters were obtained from load vs. displacement response which was measured by an extensometer.

$$\sigma_e = \frac{F}{A_o}$$

$$\varepsilon_e = \frac{\Delta L}{L_o}$$

The value of true stress and true strain can be calculated from the expression as stated in Eq. (30) and Eq. (31)

$$\sigma_t = \sigma_e(1 + \varepsilon_e)$$

$$\varepsilon_t = ln(1 + \varepsilon_e)$$

Using true stress and true strain, hollomon's equatoin is applied and the value of strength coefficient and strain hardening exponent is calculated using Eq. (32).

$$\sigma = K\varepsilon^n$$

3.4. Anisotropy calculation

To calculate the anisotropy we need to find the dimensions of the specimen. The gauge length l_g is first measured before conducting the test. The width of the specimen is measured at three different locations w_1, w_2 and w_3 and then their average w_{avg} is calculated.

After performing the test, dimensions are calculated once again. The new gauge length is measured denoted as $\bar{l}_g$ and the width of the specimen at three different location is $\bar{w}_1, \bar{w}_2$ and $\bar{w}_3$. Then the average of the new width can be calculated as $\bar{w}_{avg}$.

Now, by using the original and the new dimensions we can find the strain of the width and the strain of the length as shown in the Eq. (38) and Eq. (39)

$$\varepsilon_l = \ln\frac{\bar{l}_g}{l_g} \tag{38}$$

$$\varepsilon_w = \ln\frac{\bar{w}_{avg}}{w_{avg}} \tag{39}$$

We know from the volume consistency Eq. (36) that sum of strains in three different direction will be zero.

$$\varepsilon_l + \varepsilon_w + \varepsilon_t = 0$$

As thickness variation will be small during the test, it can be replaced by rearranging the Eq. (40) as shown:

$$\varepsilon_t = -(\varepsilon_l + \varepsilon_w) \tag{40}$$

The Lankford coefficients in the 0°, 45° and 90° direction which can be written as shown in Eq.(41) , Eq.(42) and Eq.(43)

$$r_0 = \frac{\varepsilon_w}{\varepsilon_t}, \tag{41}$$

$$r_{45} = \frac{\varepsilon_w}{\varepsilon_t}, \tag{42}$$

$$r_{90} = \frac{\varepsilon_w}{\varepsilon_t} \tag{43}$$

The Eq. (41) , Eq.(42) and Eq.(43) will be replaced in all these to form an expression given in Eq. (41) , Eq.(42) and Eq.(43) as shown:

$$r_0 = \frac{\varepsilon_w}{-(\varepsilon_l+\varepsilon_w)}, \tag{44}$$

$$r_{45} = \frac{\varepsilon_w}{-(\varepsilon_l+\varepsilon_w)}, \tag{45}$$

$$r_{90} = \frac{\varepsilon_w}{-(\varepsilon_l+\varepsilon_w)} \tag{46}$$

The Lankford coefficients for each direction are calculated three times and their average is taken which is denoted as $\bar{r}_0, \bar{r}_{45}\ and\ \bar{r}_{90}$.

The normal or the average anisotropy is calculated from the average of the Lankford coefficients and substituted in the Eq. (4).

3.5. Simulation of deep-drawing model in Ls-Dyna PrePost (R) V4.6.17

3.5.1. Geometry of the model

The geometry model of the deep drawing process was designed in LS-Dyna. The dimension of the model for sheet thickness of 1mm and blank radius of 74mm is taken according to the Figure.15. The dimension of the model will change according to sheet thickness as per the standard formulas. The model will have sheet thickness of 1mm, 1.5mm and 2mm which will also change the die clearance. The die clearance is taken according to the formula which states that die clearance should be 20% of the sheet thickness[18]. The blank radius will also change, which is varied to find the LDR of the model[75] .

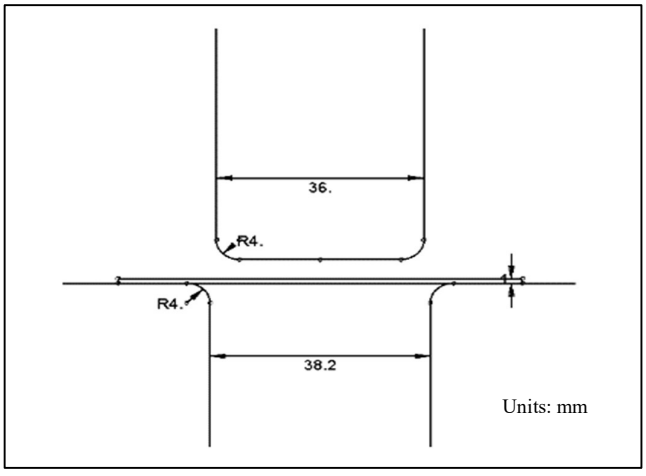

Figure.15: Deep Drawing Setup

3.5.2. Meshing of the model

After designing parts, they are then meshed with the help of an auto mesher. The sheet is meshed with an element size of 1mm and other parts like punch, and die. and the blank holder meshes with an element size of 2mm which can seen in Figure.16 a) b) c) d) below [75].

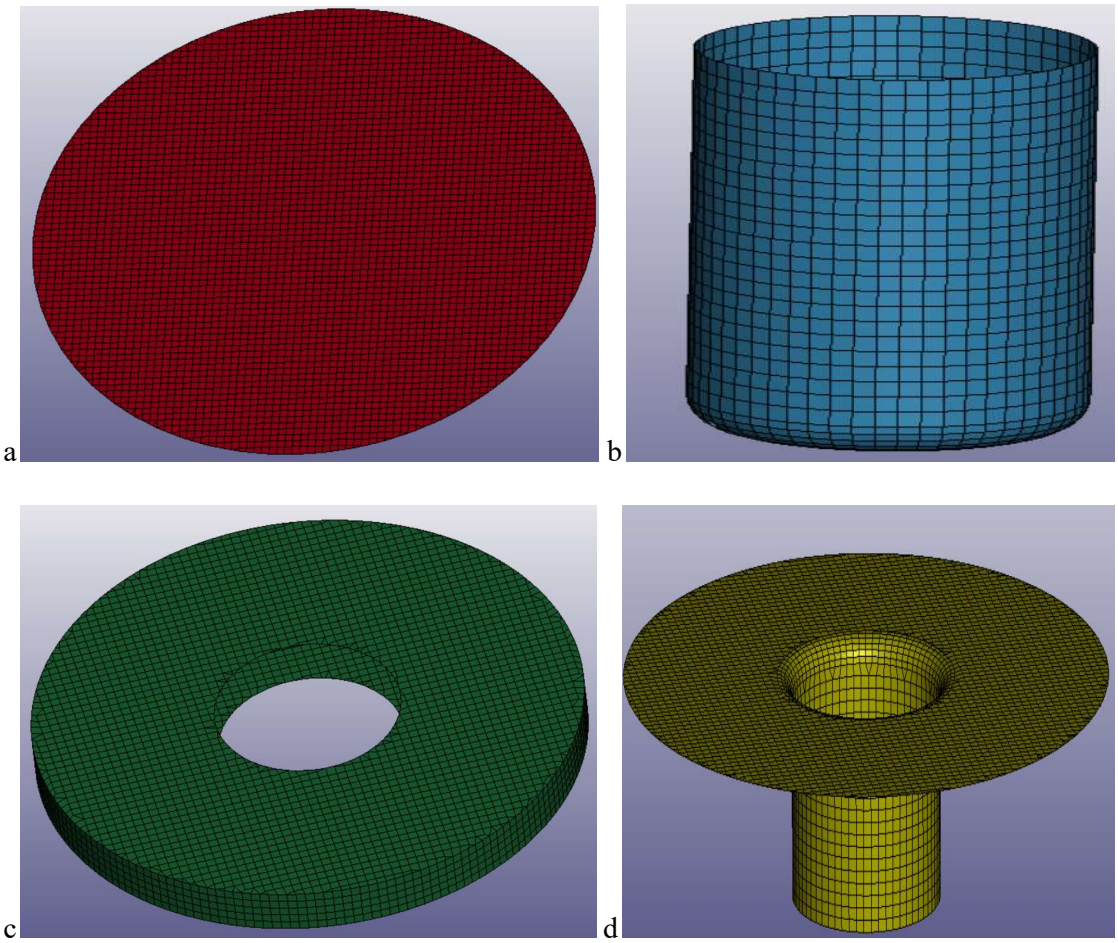

Figure.16: Meshing of parts a) Sheet b) Punch c) Blank holder d) Die

3.5.3. Sectional properties of the model

In the sectional properties, the type of shell element opted for the sheet is fully integration as the computational is very fast [75]. It is selected in option EQ 16 of the section shell as seen in the Figure.17. Here we also define our thickness as 1mm, 1.5mm, and 2mm according to the dimension of the model required. The shear factor for the sheet taken as suggested is

0.8333333. The element type in other parts is taken as the default value of 2 regarded as Belytschko-Tsay as seen in Figure.18 [75].

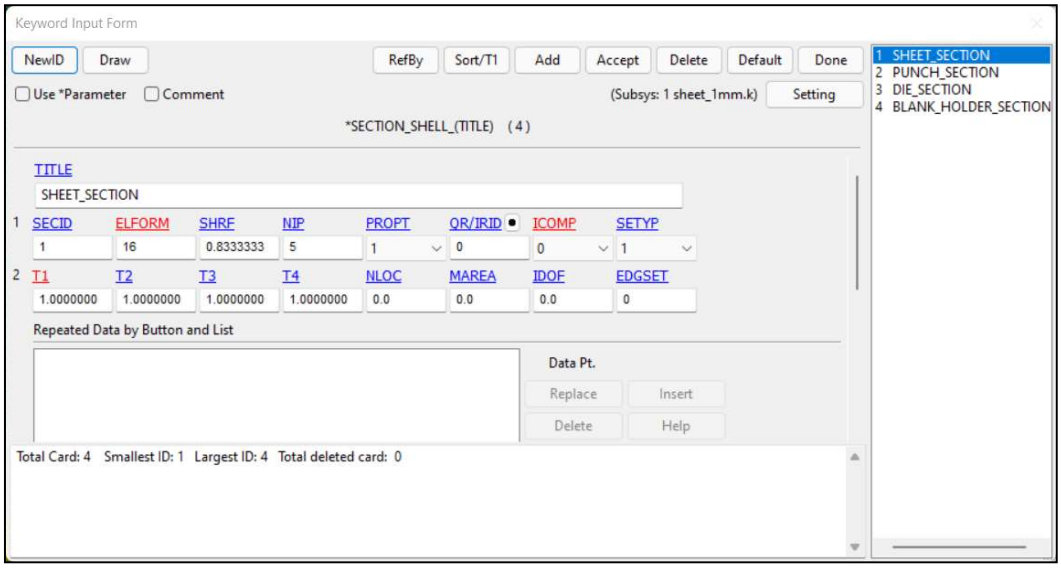

Figure.17: Section properties for sheet in a shell element with 1mm thickness

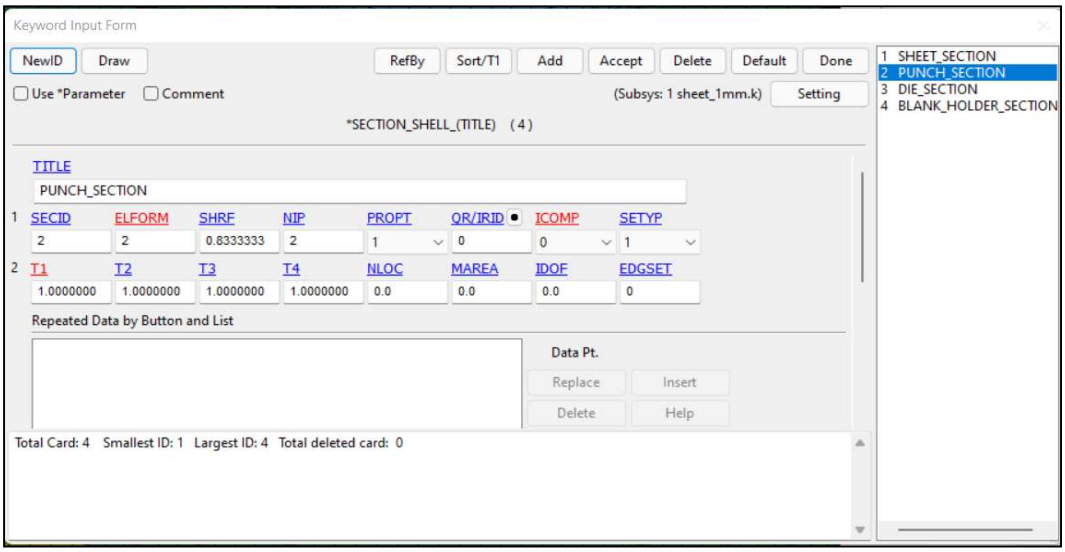

Figure.18: Section properties for a Punch and is similar for other parts

3.5.4. Selection of materials on parts

3.5.4.1. 'MAT_036': Barlat 3-parameter model for sheet

Barlat 3-Parameter is a material model for category of materials for type 36 as seen in Figure.19. Barlat and Lian [1989] presented this model which is generally used for anisotropic

material in plane stress condition for modelling sheet in the presented deep drawing process. We have given M value as 8 because aluminium is an FCC material. The hardening rule is taken as exponential as we are following Holloman's equation, so the HR value is chosen as 2. The results from the tensile test will give us the K as well as the n value. The remaining values are the standard data. The Lankford coefficients R00, R45, and R90 are calculated from the anisotropy tensile test. The parameters are tabulated in Table.2 and results in Table.3 [76].

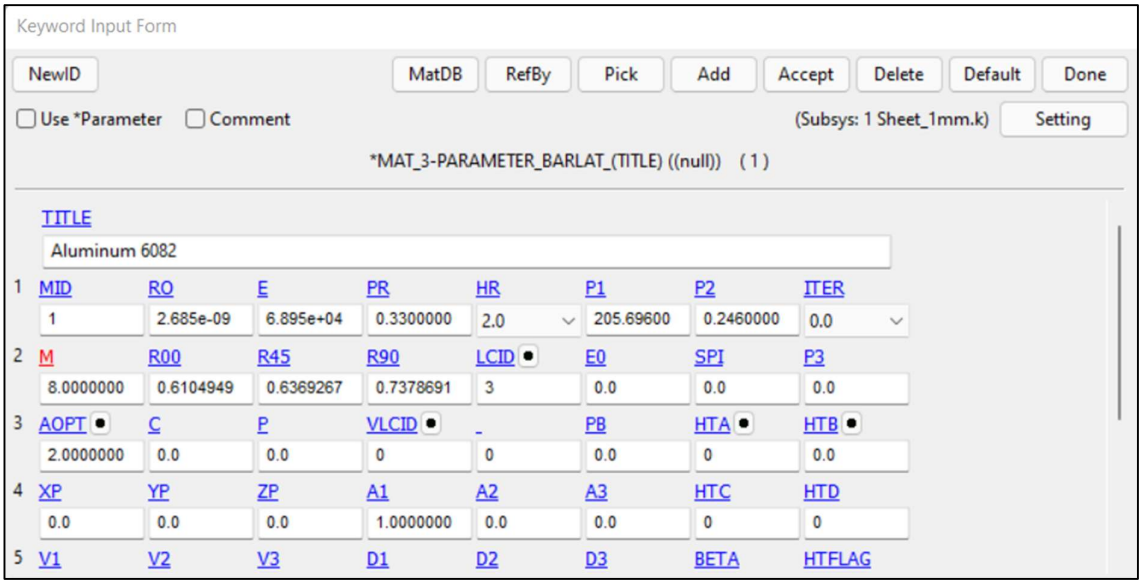

Figure.19: 'MAT_036': Barlat 3-parameter model for AA6082

Table.2: Mat_036: Barlat 3-Parameter Parameters

PARAMETERS	DETAILS
MID	Material identification (Unique Number)
RO	Mass Density
E	Young's modulus
PR	Poisson's ratio
HR	Hardening rule
	EQ.2.0: exponential
P1	Material parameter

	EQ.2.0: k, strength coefficient for exponential hardening
P2	Material parameter EQ.2.0: n, exponent
M	Exponent in Barlat's yield surface.
R00	Lankford parameter in 0° direction
R45	Lankford parameter in 45° direction
R90	Lankford parameter in 90° direction
LCID	Load curve/table ID for hardening in the 0 degree direction
AOPT	Material axes option EQ.2.0: globally orthotropic with material axes determined by vectors defined below, as with *DEFINE_COORDI_NATE_VECTOR
A1	Component of vector a for AOPT = 2.
D2	Component of vector d for AOPT = 2.

Table.3: Material properties of AA6082

ρ (Tonnes/mm^2)	Young's modulus (N/mm^2)	μ	K (MPa)	n	M (FCC)
2.685e-09	6.895e+04	0.33	205.696	0.246	8

3.5.4.2. 'MAT_RIGID' MODEL for punch, blank holder and die

This is material card 20 in Ls-Dyna where parts are said to behave as a rigid body. We have options to set a constraint in x,y,z direction as well as x,y, and z rotations.

As we know the punch and blank holder will only move in the downward direction and are constrained in the other direction. Similarly, they are also constrained to rotate in every direction. So we will apply constraint in the global direction by selecting 2 which will enable us to constraint the part in the x,y direction by selecting option 4 as well as also give us the ability to constraint in all other x,y,z, rotations by selecting option 7 as seen in Figure.20 [76].

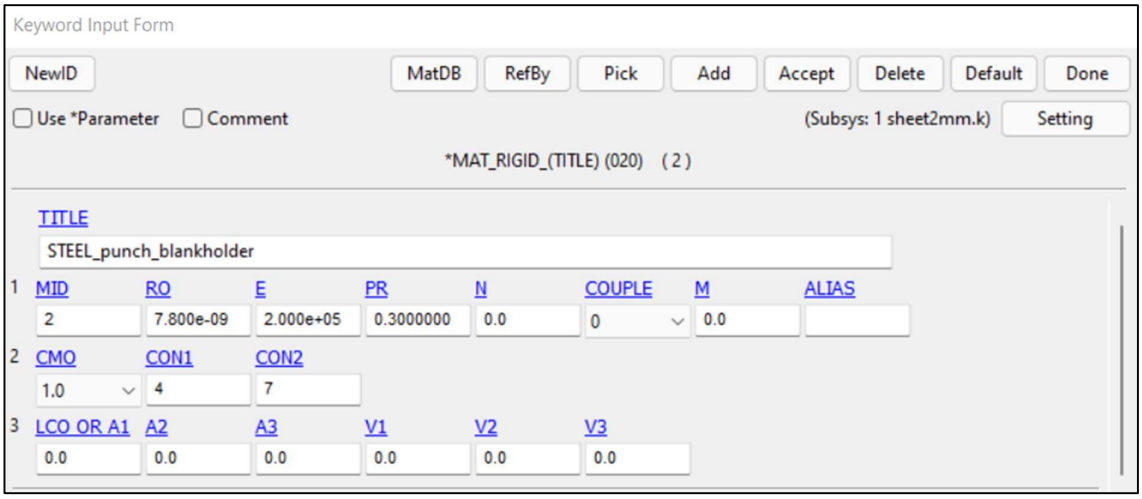

Figure.20: 'MAT_RIGID' parameters for steel punch and blankholder

Similarly, we need to fix the die in x,y,z direction as well as x,y,z rotation. So we will again select global constraints and select option 7 for both the cases to fix the die as a stationary part as seen in Figure.21 [76].

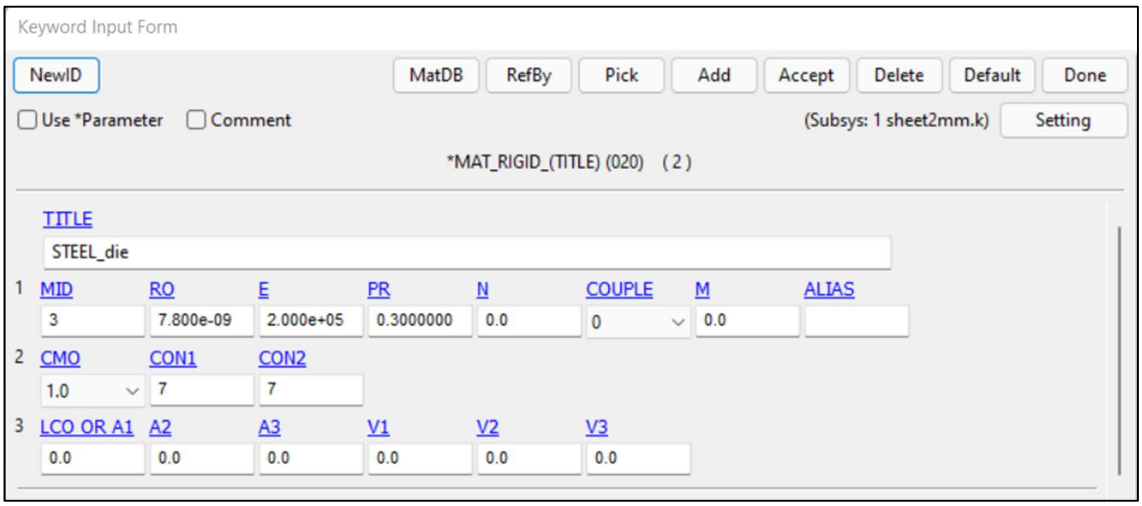

Figure.21: 'MAT_RIGID' parameters for steel die

Table.4: Mat_Rigid Parameters

MID	Material identification. A unique number has to be used.

RO	Mass density
E	Young's modulus
PR	Poisson's ratio
CMO	Center of mass constraint option EQ.+1: constraints applied in global directions If CMO=+1.0
CON1	EQ.7: constrained x, y, and z displacements, EQ.4: constrained x and y displacements If CMO=+1.0:
CON2	EQ.4: constrained x and y rotations, EQ.7: constrained x, y, and z rotations.

Table.5: Material properties for steel in punch, blankholder and die

P (T/mm^2)	Young's modulus (N/mm^2)	μ
7.8e-09	2.0e+05	0.3

3.5.5. Define Curves

3.5.5.1. Defining displacement curve of punch

The curve for the displacement of punch is defined in the define_curve card in Ls-Dyna [75]. The displacement curve in Figure.22 is calculated for 3000 mm/s. Similarly, we will define the displacement curves for other speeds like 4000 mm/s and 5000 mm/s. The constant displacement curve is plotted in the Figure.23.

Now, to define constraints or boundary conditions of the punch we will use 'Boundary prescribed motion rigid' card as shown in Figure.24. We will specify the Degree of freedom (DOF) at a value of 3 which only permits movement in the z-direction. In all the other directions the punch is constraint and cannot move. VAD (Velocity, Acceleration, and displacement) option in the prescribed motion rigid card is utilized to select the type of motion and we will select displacement as we have earlier defined displacement curve. The scale factor is chosen as -1 because the movement of the punch is in the negative or downward direction.

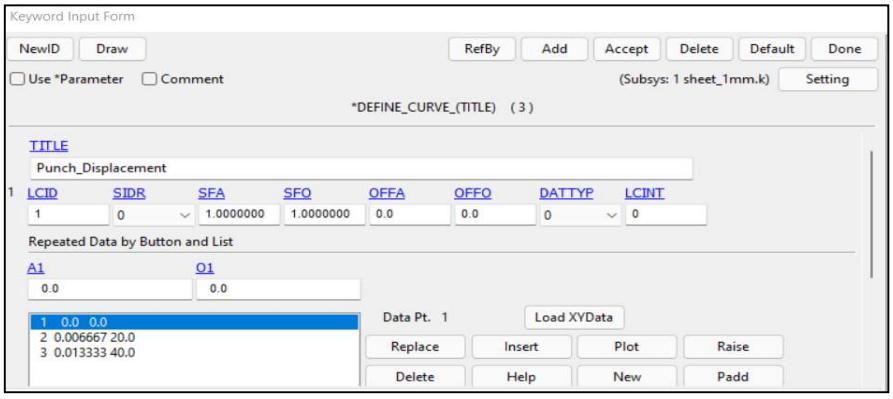

Figure.22: Defining curve of punch

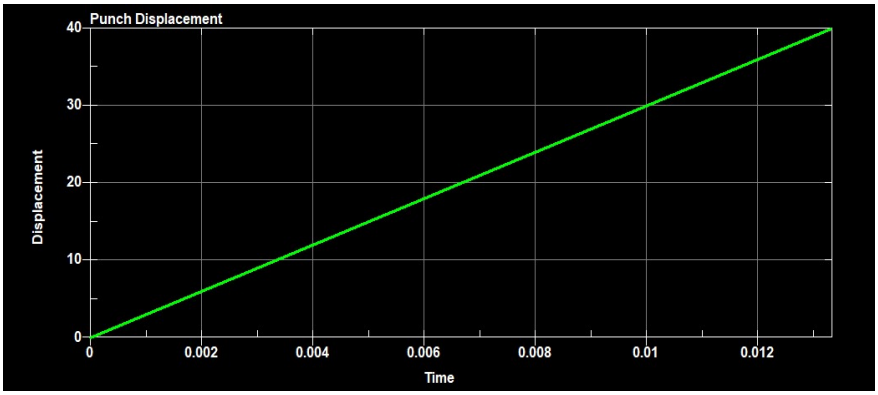

Figure.23: Constant punch speed curve for 3000 mm/s

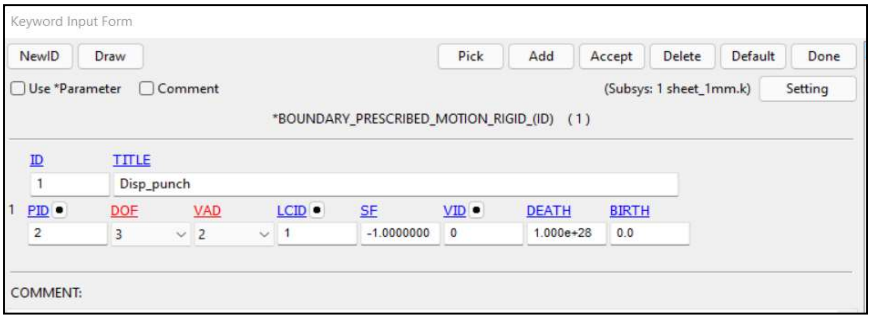

Figure.24: Defining boundary conditions for a punch

3.5.5.2. Defining load curve for blank holder

To fix the sheet between die and blank holder we need to apply load on the blank holder so that it will press the sheet against the die. Therefore, to apply load we need to define load curve. The load on a blank holder or the blank holding force (BHF) in deep-drawing operation is calculated by the standard formula given in Eq.(47).

$$BHF = 2\% * \left(\frac{\sigma_y + \sigma_{UTS}}{2}\right) \quad (47)$$

The calculated BHF is applied in the curve as shown in the Figure.25 and the curve is plotted between BHF and time is shown in the Figure.26.

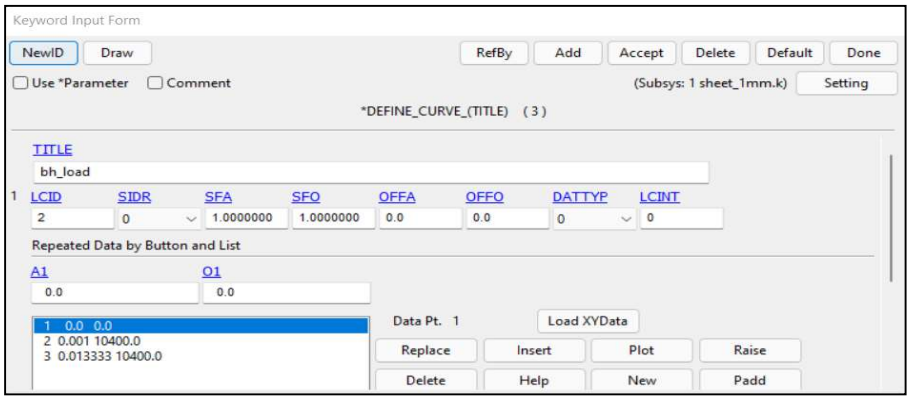

Figure.25: Defining curve of load on the blank holder

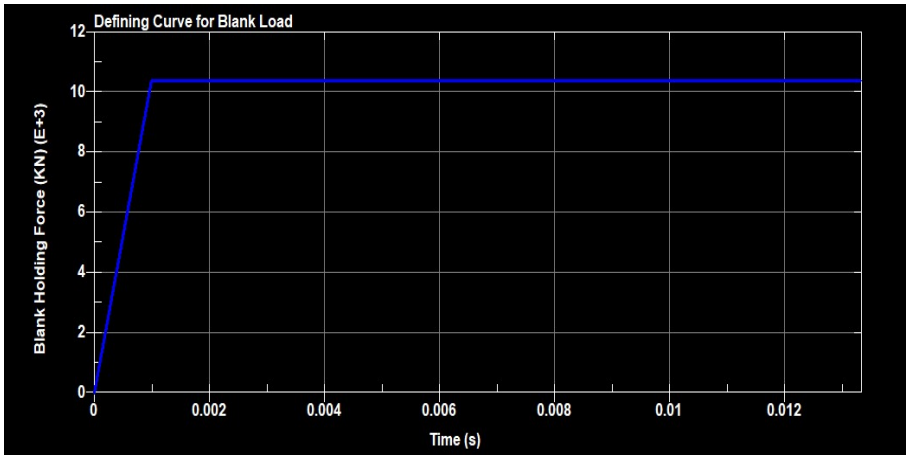

Figure.26: Curve for Blank holding force value of 10.4 KN

Now, after defining the curve we need to apply the load and also provide required constraints. The 'Load Rigid Body' card in Ls-Dyna as shown in Figure.27 is used to apply the curve as well as constraints [75]. The DOF will be selected to be 3 as we want blank holder to be moving in the z-direction only, rest all directions will be constraints. LCID is used to select and apply the load curve which we have already defined. The scale factor here also is -1 to denote negative or downward direction of load.

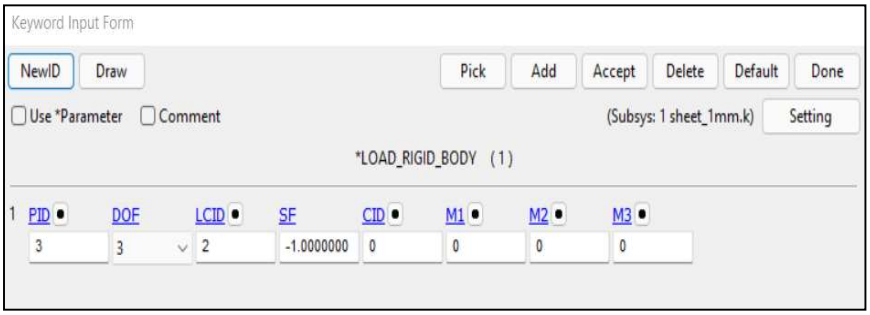

Figure.27: Defining boundary conditions for blank holder load

3.5.5.3. Defining Stress-Strain curve of AA6082 material

The curve of the True stress-True strain is defined for AA6082 material as shown in the Figure.28 and its subsequent graph is plotted in the Figure.29. This curve will be applied on the Barlat 3 parameter model by using LCID option [75].

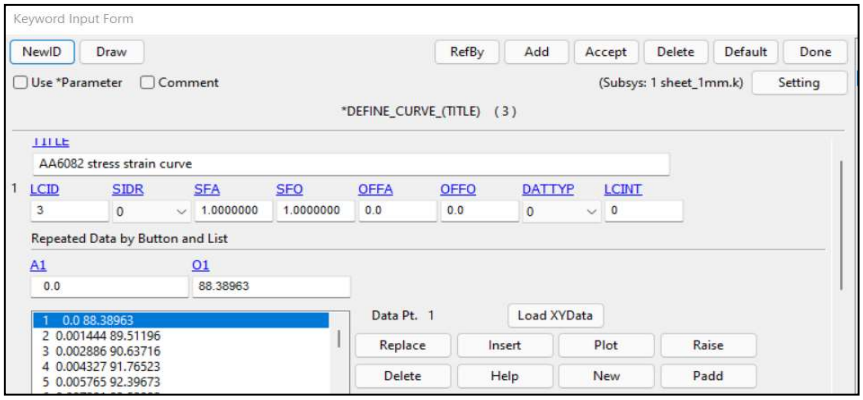

Figure.28: Defining stress-strain equation of AA6082 material.

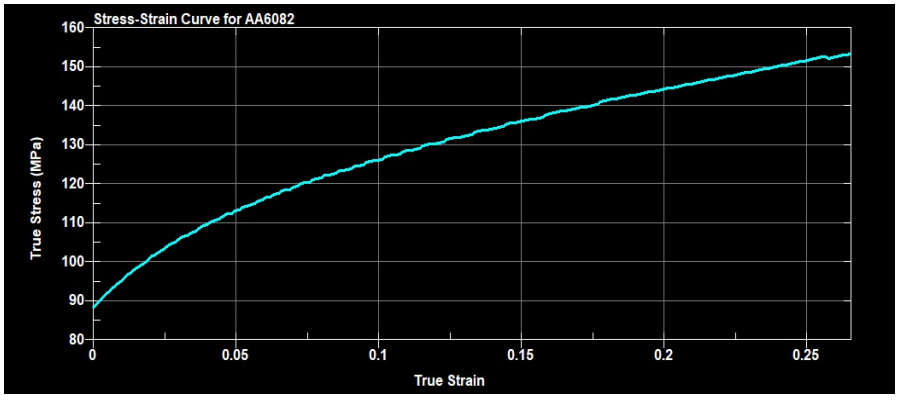

Figure.29: Plotting stress-strain equation of AA6082 matrerial

3.5.6. Defining contacts between parts

We need to define contacts between parts so that they identify each other. The type of contact we are using here is 'CONTACT_FORMING_ONE_WAY_SURFACE_TO_SURFACE' [75].

While defining contacts selecting master and slave part is an important step. Here in deep drawing process, sheet is always taken as a slave segment and other parts like punch, die and blank holder is taken as master segment as shown in Figure.30, Figure.31 and, Figure.32. SSID is the slave segment ID and MSID is the master segment ID.

We can also define friction in between parts in this contact card. FS represents static friction and FD represents dynamic friction between contacts. The static friction between die and sheet is varied from 0.1, 0.15 and 0.2.

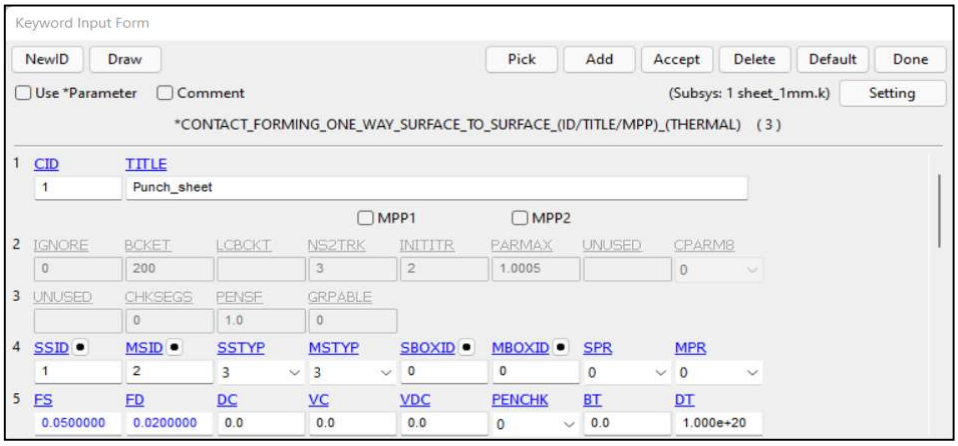

Figure.30: Contact between punch and sheet

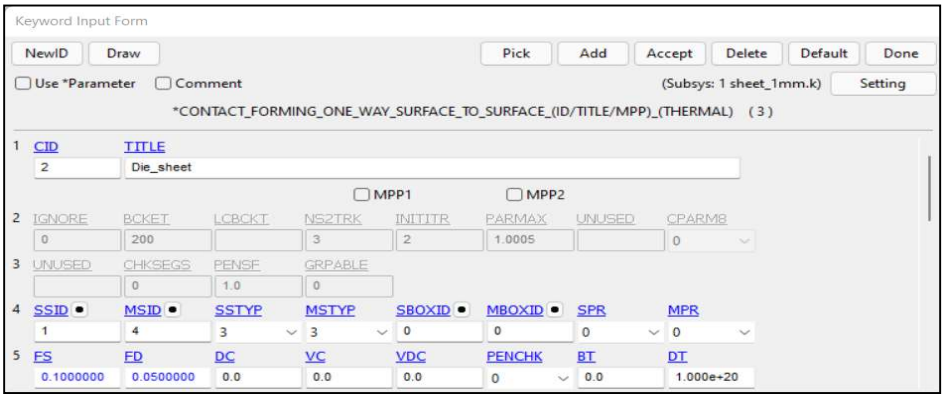

Figure.31: Contact between Die and sheet

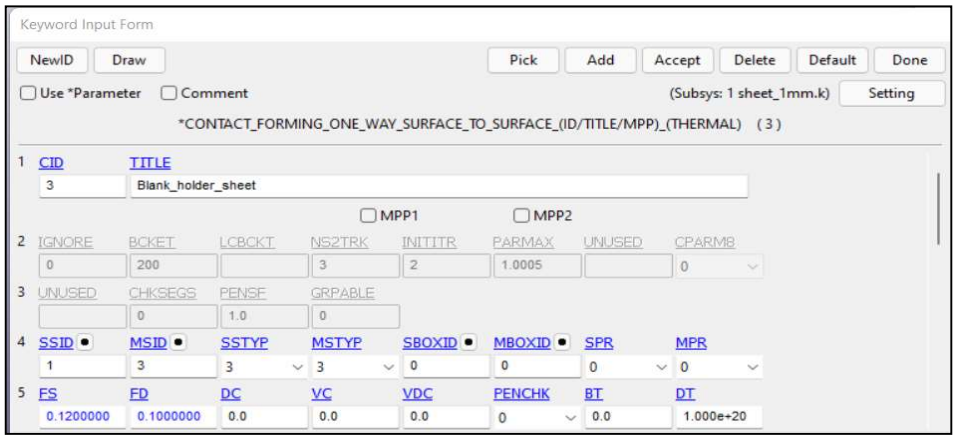

Figure.32: Contact between Blank Holder and sheet

3.5.7. Setting control and database card

The 'DATABASE_BINARY D3PLOT' card in database as seen in Figure.33 is most import card which is used to set the time interval between the outputs referred as 'DT' [75]. We have set DT to a value of 0.0001.

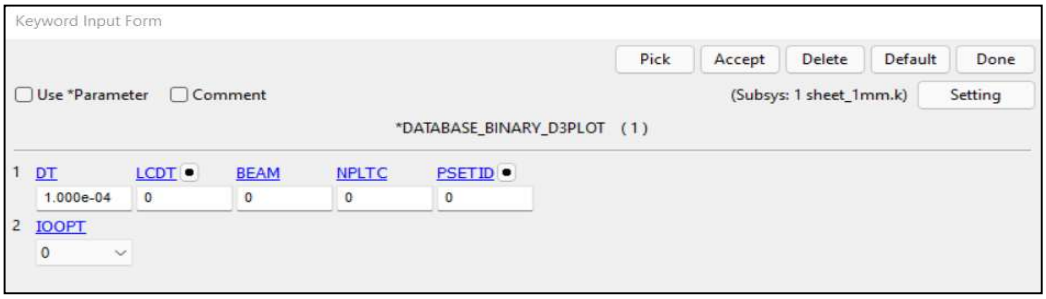

Figure.33: Setting Interval time in 'BINARY_D3_PLOT'

In the control option, setting up termination time of simulation is vital as seen in Figure.34.

Figure.34: Setting termination time in 'CONTROL_TERMINATION' card

The change in thickness properties in shell element is obtained after setting up the 'Control shell' card as shown in Figure.35. The ISTUPD option is set to 1 which will take care of all the thickness change in the parts. This card is useful in the sheet metal operations whenever there is stretching or membrane change [75].

Figure.35: Setting up Shell thickness change in 'CONTROL_SHELL' card

3.6. IDENTIFICATION OF JC PARAMETERS

A number of tensile tests were performed on the UTM machine to obtain Stress-Strain readings. The test was carryout out at varied strain rates of 10^{-4} s^{-1}, 10^{-3} s^{-1}, 10^{-2} s^{-1}, and 10^{-1} s^{-1} and also at different temperatures at 50°C, 100°C, 150°C, and 200°C.

3.6.1. Determination of A, B and n Parameter

The readings from UTM machine is used to find the true stress and true strain using Eq. (30) and Eq. (31) . On the graph we will draw a 0.2% offset line which will cut the true stress and true strain curve. The point where the offset line cuts the graph is the A parameter or yield point at the deformation taken at reference condition.

We know that from Eq. (36),

$$\sigma_e = \left(A + B\varepsilon_p^n\right)\left(1 + Cln\frac{\dot{\varepsilon}}{\dot{\varepsilon_o}}\right)(1 - T^{*M})$$

Now, if the readings are taken at room temperature and reference strain rate 10^{-3} s^{-1}, the second and third bracket brackets in Eq. (36) get equated to unity and then the Eq. (36) get reduced to the following form given by Eq. (48),

$$\sigma_e = \left(A + B\varepsilon_p^n\right) \quad (48)$$

We are conducting uniaxial tensile test therefore,

$\sigma_e = \sigma$ and $\varepsilon_p^n = \varepsilon$

Eq. (48) now becomes,

$$\sigma = (A + B\varepsilon^n) \tag{49}$$

If we take log on both sides, the Eq. (49) becomes

$$\log(\sigma - A) = \log B + n \log \varepsilon \tag{50}$$

'A' value is put in this Eq. (50) and then the graph between $\log(\sigma - A)$ Vs $\log \varepsilon$ is plotted. The value of B will be provided by the intercept on the y-axis and the n value is given by the slope of the curve [77].

3.6.2. Determination of C Parameter

To determine the C Parameter, we will conduct the experiment at different strain rate. The stress-strain curves will be at different strain rates but the temperature will be at room temperature so the third bracket in the Eq. (36) will become unity and the Eq. (36) will get reduced to Eq. (51):

$$\sigma_e = \left(A + B\varepsilon_p^n\right)\left(1 + Cln\frac{\dot{\varepsilon}}{\dot{\varepsilon_o}}\right) \tag{51}$$

which can also be written as Eq. (52),

$$\frac{\sigma_e}{(A+B\varepsilon_p^n)} = (1 + Cln\dot{\varepsilon}^*) \tag{52}$$

Where, $\dot{\varepsilon}^* = \frac{\dot{\varepsilon}}{\dot{\varepsilon_o}}$

To get the C parameter we have to now plot the curve between $\frac{\sigma_e}{(A+B\varepsilon_p^n)}$ and $ln\dot{\varepsilon}^*$. The slope will give us the C parameter after we draw a trend line on the curve. The reference strain rate was taken as 10^{-3} s^{-1}

3.6.3. Determination of m Parameter

To find the m parameter we will find the readings at different temperatures and the reference temperature was taken was the room temperature. The second bracket from Eq. (36) will be

equal to unity as reference strain rate was used to conduct the experiment[78]. The Eq. (36) will not be get reduced to given by Eq. (53):

$$\sigma_e = \left(A + B\varepsilon_p^n\right)(1 - T^{*M}) \tag{53}$$

We have taken the first value as it represents the reference condition. Then the Eq. (53) can be also written as Eq. (54),

$$1 - \frac{\sigma_e}{(A+B\varepsilon_p^n)} = (1 - T^{*M}) \tag{54}$$

Taking log on both the sides to give Eq. (55) ,

$$\ln\left(1 - \frac{\sigma_e}{(A+B\varepsilon_p^n)}\right) = M \ln(T^*) \tag{55}$$

Now, the graph is plotted between '$\ln\left(1 - \frac{\sigma_e}{(A+B\varepsilon_p^n)}\right)$ Vs $\ln(T^*)$ ' and a trend line is drawn on the curve to get the slope of the curve. The slope represents the M parameter[77].

CHAPTER 4

RESULT AND DISCUSSION

4.1. Determination of Stress Strain curve of AA6082-T6

Initially the AA6082-T6 material is tensile tested on a UTM machine. The force and positions data is obtained from the test which is used to find the true stress vs. true strain data. This data will be used to draw true stress-true strain graph which gives us yield stress and ultimate tensile stress as shown in the Figure.36. They yield stress and ultimate tensile stress was found to be 276.5353822 and 323.6053719 respectively. The strain was found to be 5%-6%.

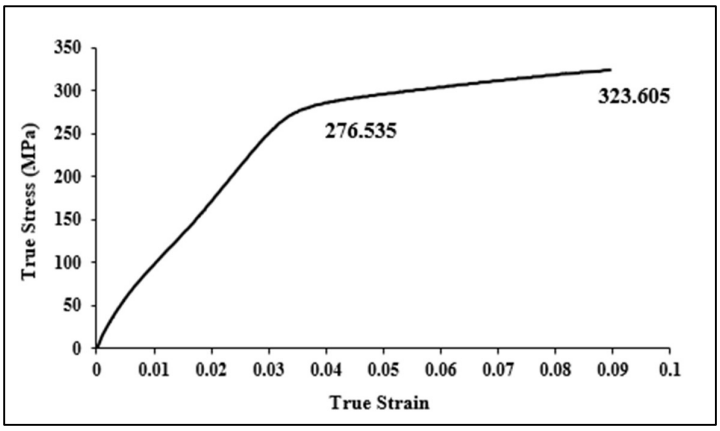

Figure.36: True Stress Vs True Strain of AA6082-T6

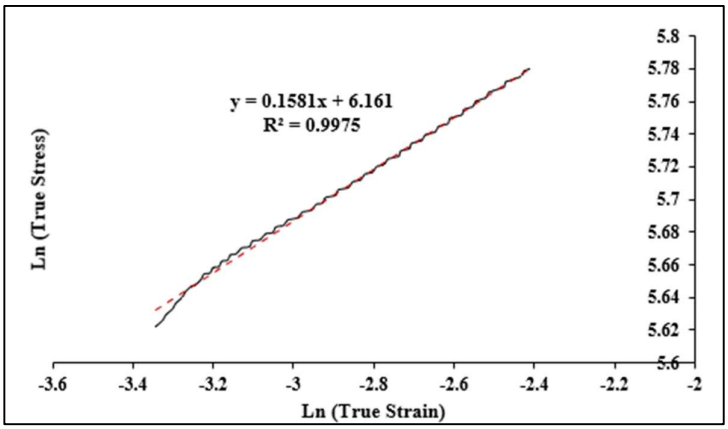

Figure.37: Ln True Stress Vs Ln True Strain of AA6082-T6

Then ‘Ln True Stress Vs Ln True Strain’ graph was plotted as depicted in the Figure.37. From these reading ‘K’ and ‘n’ values were found out to be 666.0735 and 0.2628 respectively.

4.2. Annealing of AA6082

To attain higher elongation, we need to anneal the material which we achieve in an industrial muffle furnace as seen in the Figure.38. In the furnace, sand is first poured in a metallic holder and then it is heated to remove the moisture present in it. After removing moisture from the sand, material is placed inside the sand. Then the temperature of the furnace is increased from 200°C till 350°C as shown in Figure.39 a) b) c) d).

Figure.38: Industrial Muffle Furnace

Figure.39: a) 200°C Temperature b) 250°C Temperature c) 300°C Temperature d) 350°C Temperature

4.3. Determination of Stress Strain curve ofAA6082-O

After annealing the material, again the tensile test is performed on the test piece. The various readings were noted down in excel sheet. From that sheet we repeat the process of finding true stress and true strain. It is clearly observed from Figure.40 that the elongation increased by 15% and ductility of the material is increased after annealing.

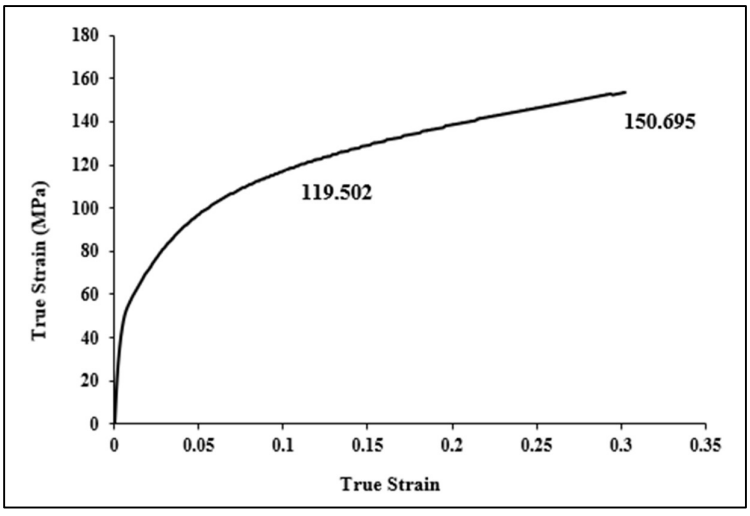

Figure.40: True Stress Vs True Strain of AA6082-O

Then again, we plotted 'Ln True Stress Vs Ln True Strain' graph as shown in Figure.41. This time K and n value was observed to be 205.696 and 0.246 respectively

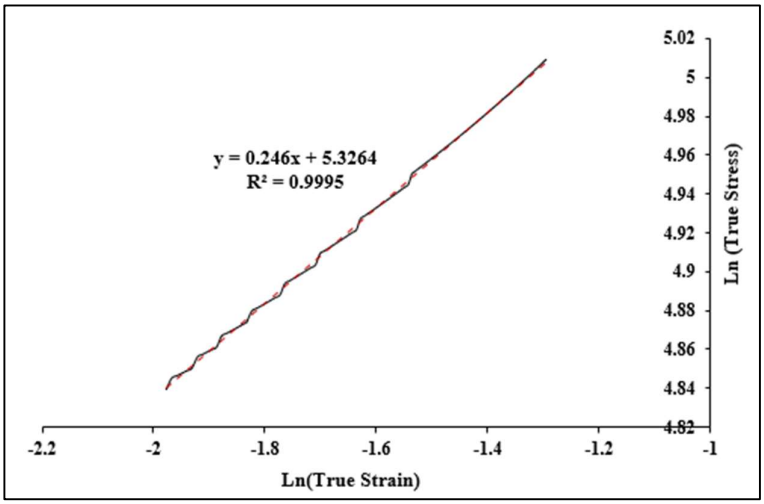

Figure.41: Ln True Stress Vs Ln True Strain AA6082-O

4.4. Anisotropy Results of AA6082

The anisotropic results are calculated and tabulated in Table 6.

Table.6: Anisotropic Results

No of Experiments	**Readings**	r_{avg}	r_m
0-Aniso-1	0.636591		
0-Aniso-2	0.691088	0.610495	
0-Aniso-3	0.503806		
45-Aniso-1	0.692304		
45-Aniso-2	0.648892	0.636927	0.655554
45-Aniso-3	0.569584		
90-Aniso-1	0.635211		
90-Aniso-2	0.866719	0.737869	
90-Aniso-3	0.711677		

4.5. Effect of blank position during sheet deformation on sheet deformation

The position of blank between the die and the blank-holder has a prominent effect on the strain rate during sheet deformation. As we shift our blank to one side, there will be increase in the sheet material on one side of flange and the other side will see decrease in sheet material. The location which has more area of sheet material will undergo resistance to flow while the location where there is less material undergoes less resistance. As we can see in the Figure.42 a) , with 0.2 mm blank offset there is a increase in material on one side than the other side. With more increase in blank offset there comes a time the shape of the cup gets distorted and there is a more than sufficient increase in flange and other side experience unusual deformation as seen in the Figure.42 b)

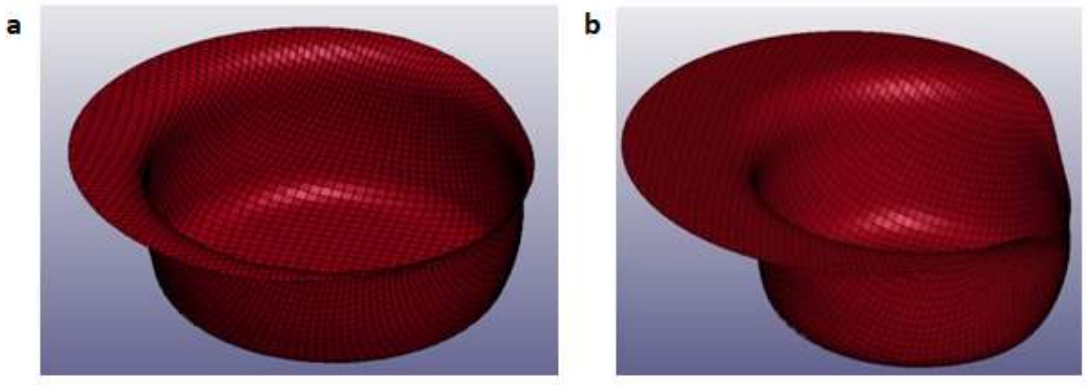

Figure.42: a) 0.2 mm blank offset resulting in increase of one side of flange material b) 0.5mm offset resulted in unusual and incomplete deformation

4.6. Variation of thickness during sheet deformation

4.6.1. Thickness at flange for different sheet thickness

The flange region experiences two opposite natures of stress namely hoop or circumferential stress and radial stress. So, the nature of the load is tensile in the radial direction and compressive in the circumferential direction. As a result, thickness in the area flank region increases as seen in Figure.43, Figure.44 and, Figure.45. The second zone of deformation is

the transition between the wall of the cup and the radius of punch profile. The region undergoes uniform axial stretching which will lead to thinning in this portion

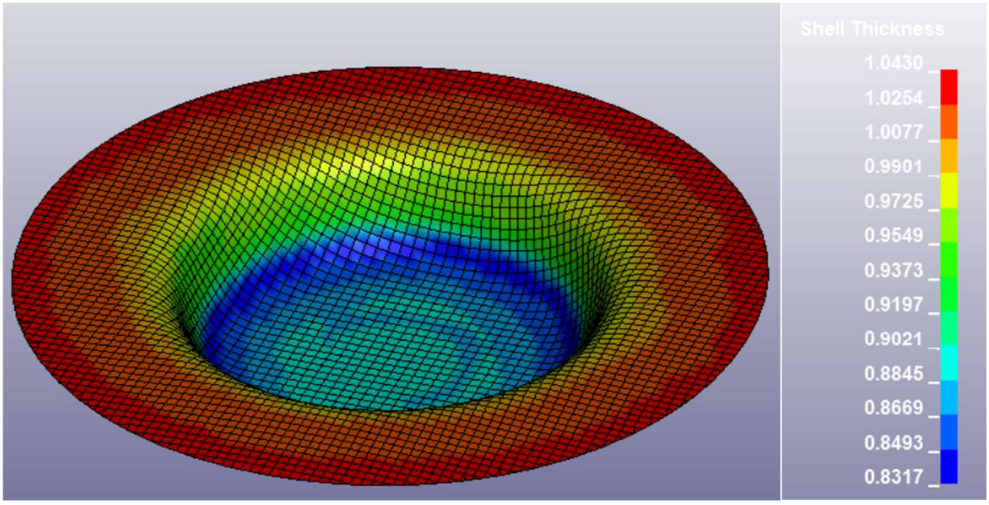

Figure.43:Flange thickness varation on a sheet of 1mm

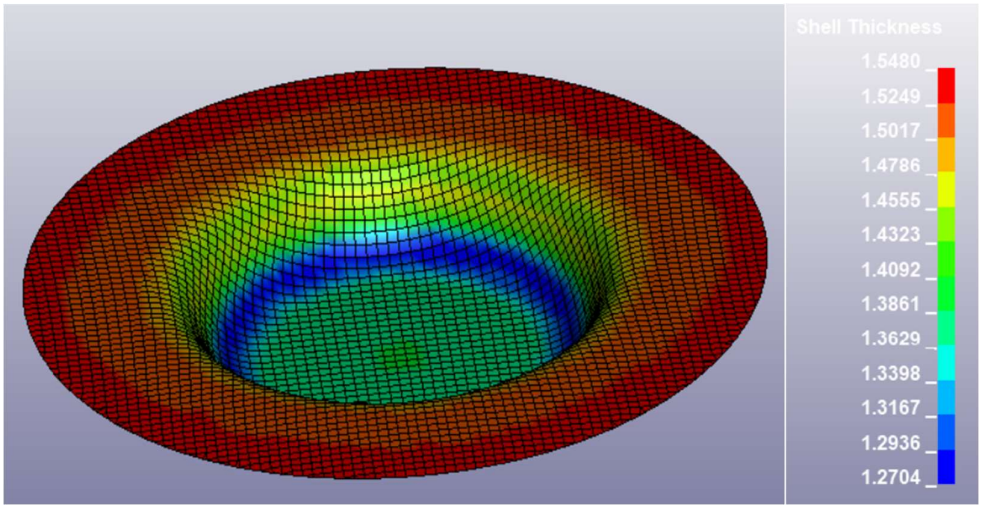

Figure.44: Flange thickness varation on a sheet of 1.5 mm

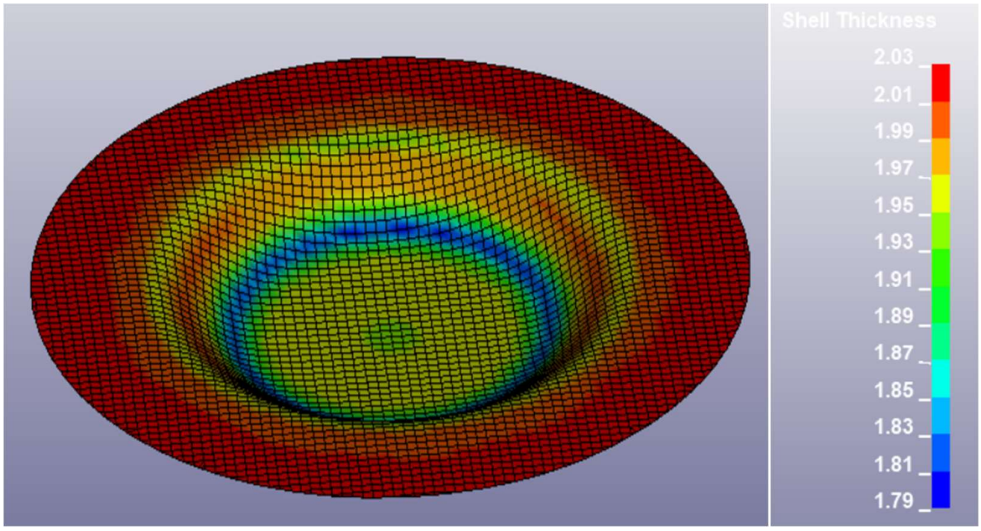

Figure.45: Flange thickness varation on a sheet of 2 mm

4.6.2. Wall thickness during sheet deformation at various coefficients of friction

The sheet thickness after deep-drawing operation can be seen in figures. It is clearly visible that with the rise in coefficient of friction there is decrease in sheet thickness at the wall section. If we consider only the wall, the thickness is reduced to 0.9753 at μ =0.1 in Figure.46, 0.9631 at μ =0.15 in Figure.47, 0.9604 at μ =0.2 in Figure.48, and 0.8869 at μ =0.25 in Figure.49. If we increase in coefficient of friction any further more it will result in necking and eventually failure due to severe reduction in thickness.

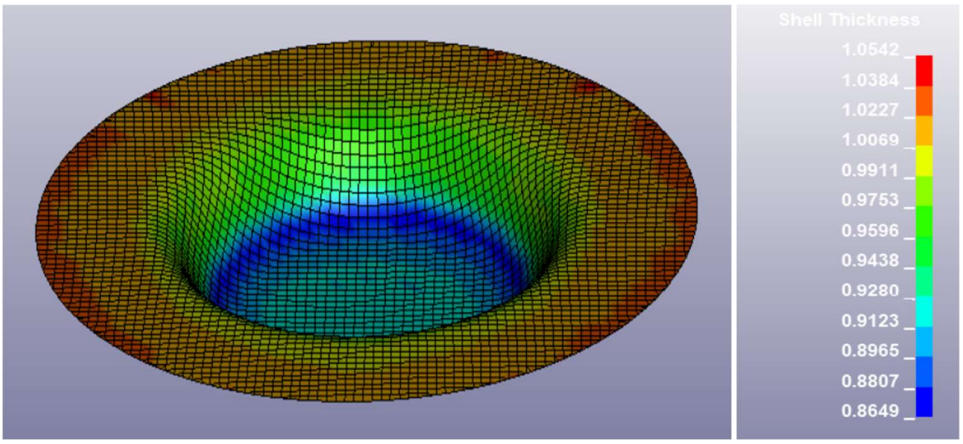

Figure.46: Wall thickness at μ =0.1

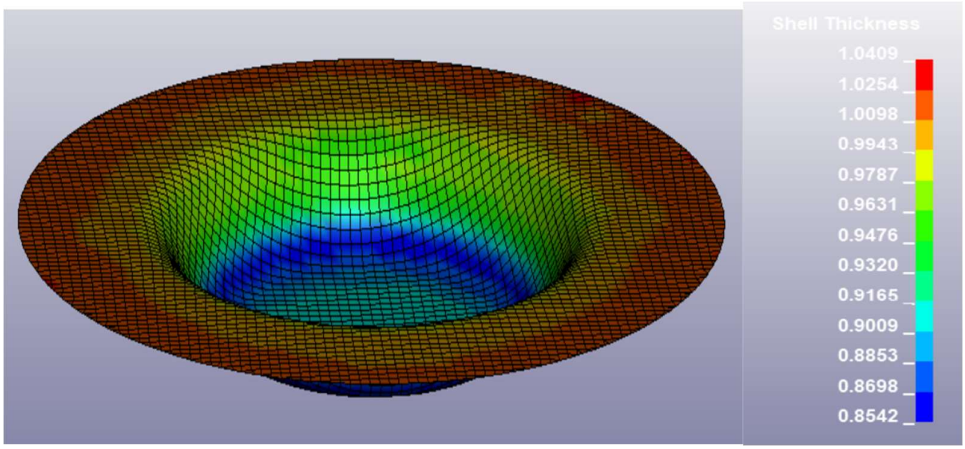

Figure.47: Wall thickness at μ =0.15

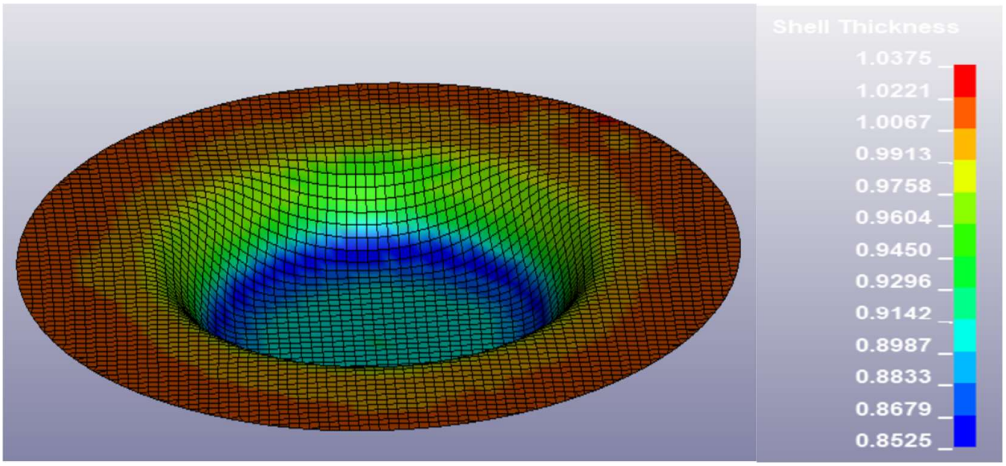

Figure.48: Wall thickness at μ =0.2

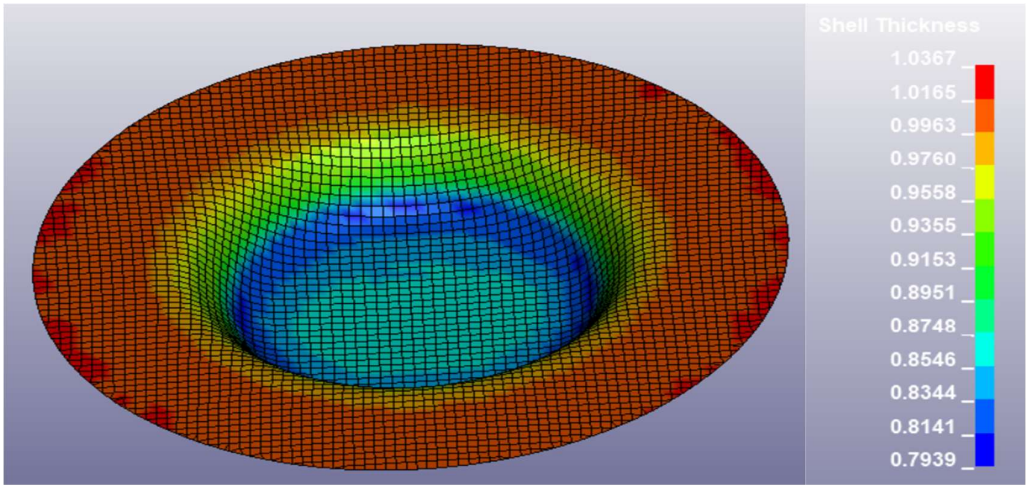

Figure.49: Sheet thickness at μ =0.25

4.7. Blank holding force during sheet deformation

We already know that blank holding force is required to eliminate wrinkling or buckling. In the figure, cups were drawn at different blank holding force for sheet thickness of 1mm and 1.5mm. For sheet of 1mm, wrinkling was seen at 0.75 kN of BHF and as we increase the BHF to 0.8 kN wrinkling was not seen as seen in Figure.50 a) b). Now for sheet of 1.5mm, we observe wrinkles at BHF of 0.52 kN and wrinkles was prevented at BHF of 0.55 kN as seen in Figure.51 a) b) .We can clearly see that as we decrease the sheet thickness there is an increase in blank holding force required to remove wrinkling.

a) Sheet thickness 1mm

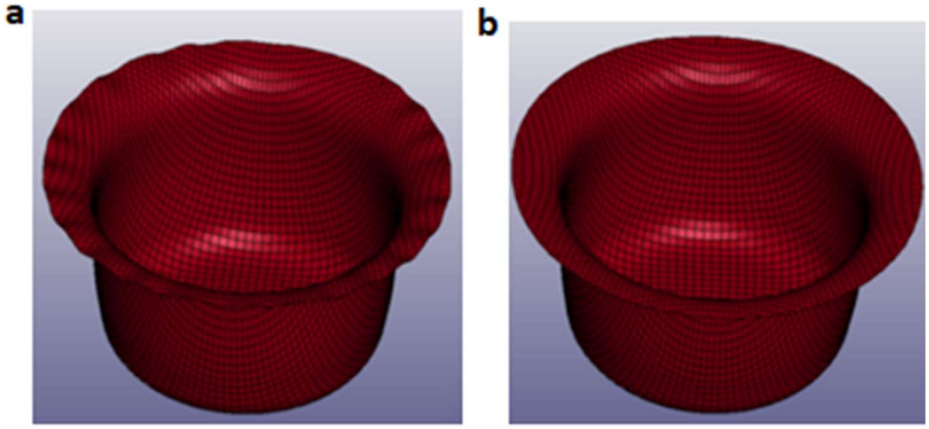

Figure.50: a) Wrinkling at BHF of 0.75 kN b) No wrinkling at BHF of 0.8 kN

b) Sheet thickness 1.5mm

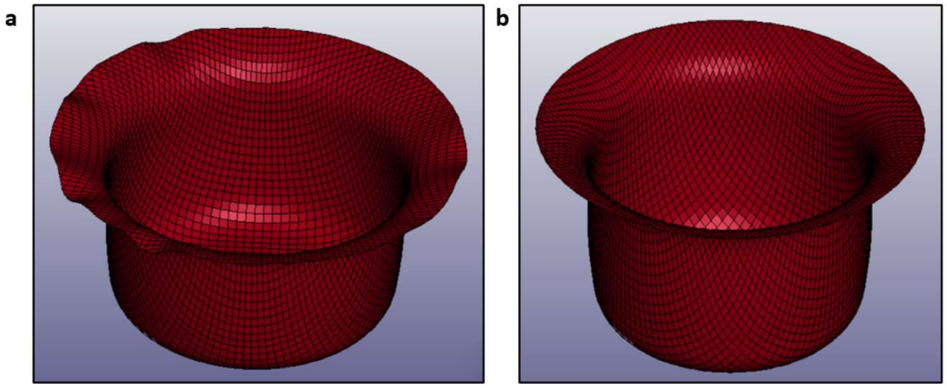

Figure.51: a) Wrinkling at BHF of 0.52 kN b) No wrinkling at BHF of 0.55 kN

4.8. Effect of r-value on Isotropic and Anisotropic material

The force which is required to deform the flange material decreases if the r value is increased. Increasing the value of r also strengthens the wall of the drawn cup. As the r-value gets higher, there is resistance to thinning as an ability of the material. The high drawing ability of material which is observed at high r value has a property that flow of material occurs only in the planer direction rather than the thickness direction. Therefore LDR increases with a high value of r.

In case of materials like aluminium the value of $r < 1$. With a less r-value the flow of material in addition to planer direction also flows in the thickness direction. This behaviour has a severe effect as there is always a tendency to thinning during deep drawing under the action of tension which can lead to failure if the thinning is more than 20%. So in a material like aluminium where there is anisotropic effects has a less r-value, therefore the LDR is less and earing are visible seen in Figure.52: b). Whereas in isotropic material R=1 as all the Lankford coefficients is equal to 1 which suggests that material flows in plane only rather than thickness direction. Therefore, material doesn't get thinner after drawing instead it gets narrower and hence drawability increases. The planer anisotropy in case of isotropic material is also zero from the formula and hence earing is not visible on isotropic materials as seen in Figure.52 a). The LDR in case of isotropic material came out to be 2.11 which was 1.969 in case of anisotropic material.

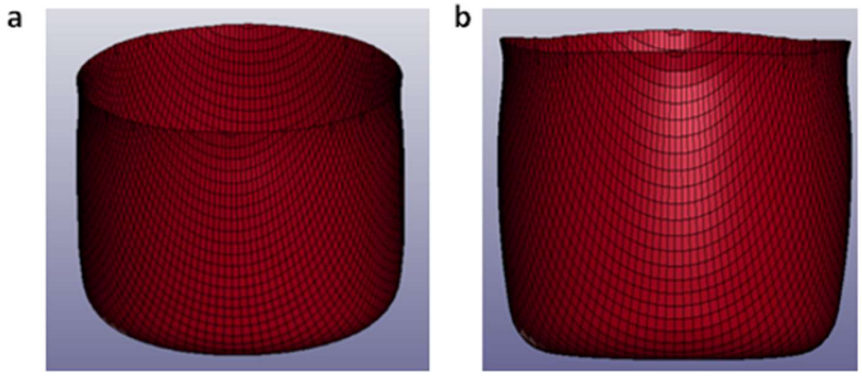

Figure.52: a) Isotropic material b) Anisotropic material

4.9. Determination of LDR at various process parameters for Barlat-3 parameter model

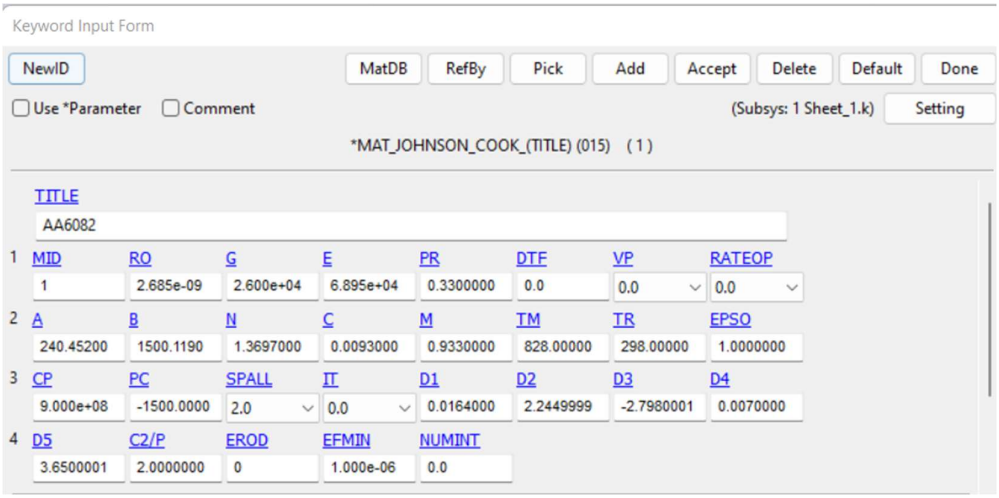

4.9.1. Variation of LDR with Sheet Thickness

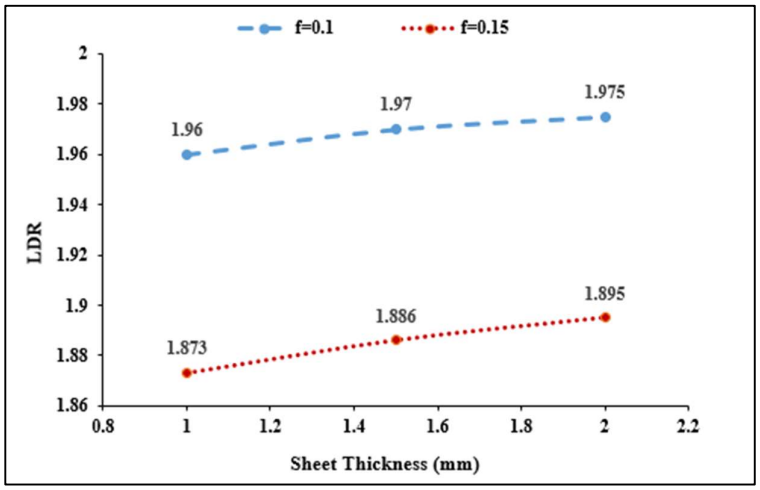

Figure.53: Variation of LDR with Sheet Thickness

In the Figure.53 we can see a curve drawn between LDR and sheet thickness. The different sheet thickness that was taken were 1, 1.5 and 2mm. At every particular sheet thickness, LDR

was found. The LDR was noted and then plotted with sheet thickness. It was found that with the addition in sheet thickness the LDR increases. As the thickness of the material decrease, the load carrying capacity of the material also decreases. Therefore, it is difficult with the decrease in thickness of sheet metal to avert failure. With the increase in thickness in sheet, stiffness also increases which is related to buckling. As a result, wrinkles are supressed on the walls and there is an increase in LDR. The readings were also taken at coefficient of friction μ =0.1 and 0.15. It was found that with increase in friction LDR decreases as we increase the sheet thickness.

4.9.2. Variation of LDR with Punch Speed

We can see in the Figure.54, the curve between LDR and speed is plotted. The speed which we have considered are 3000 mm/s, 4000 mm/s , and 5000 mm/s. At different speed, particular LDR value was calculated. We can observe that as the speed value increases from 3000mm/s to 5000mm/s, the calculated LDR decreases. The calculations were performed on 1 mm sheet.

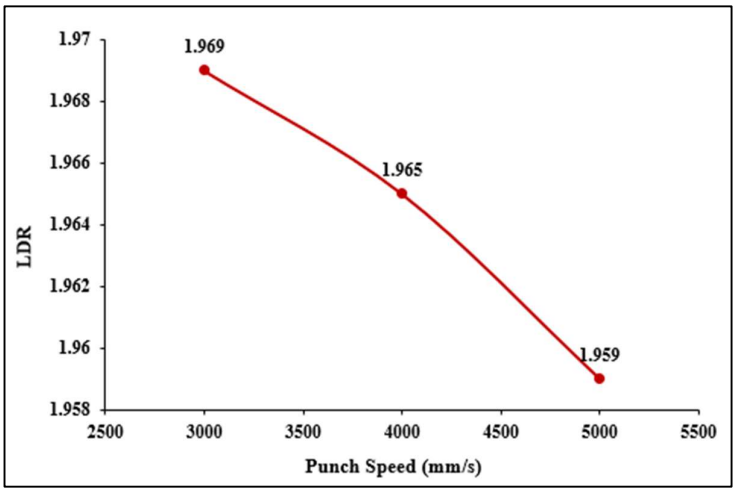

Figure.54: Variation of LDR with Punch Speed

4.9.3. Variation of LDR with BHF

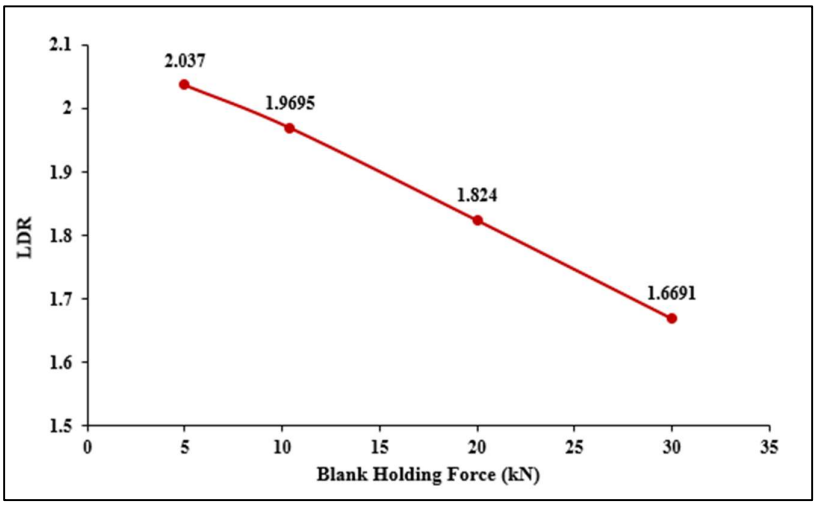

Figure.55: Variation of LDR with BHF

The blank holding force is required to prevent wrinkling on the flange as well as the wall region. In the Figure.55 the graph between LDR and blank holding force is drawn. The various BHF values taken were 5kN, 10.4kN, 20kN and 30kN. After finding values of LDR at different BHF it was seen that LDR values decreases with increase in BHF. If he BHF is of less value, more material will be drawn in thereby stresses reduces on the wall surface. As we increase the BHF, it prevents the excess flow of material and stress values increases. Therefore, as we have low value of BHF there will be deeper cups drawn and the value of LDR increases, vice versa.

4.9.4. Variation of LDR with Coefficient of friction

4.9.5. Variation of LDR with Coefficient of friction between Sheet-Die

The variation of LDR was plotted in the Figure.56 with increasing coefficient of friction between sheet and die. The value of LDR for 0.1 was 1.969, 0.15 for 1.873 and 0.2 for 1.784 and 0.25 for 1.706. We can observe that with the increase in coefficient of friction between sheet and die, LDR decreases. It can be inferred from the fact that as we increase the friction between sheet and die there is a resistance to motion. As the punch load increase and the sheet impending movement, tendency to necking increases which results in increase in thinning on the wall of the cup hence drawability decreases.

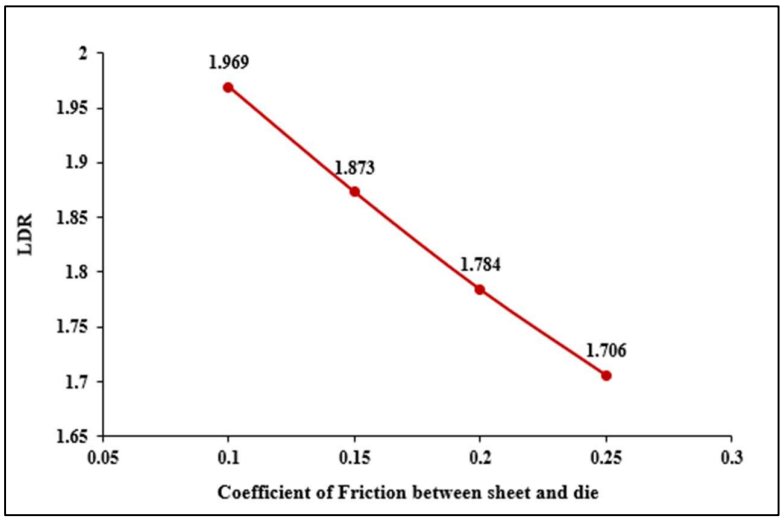

Figure.56: Variation of LDR with Coefficient of friction between sheet and die

4.9.6. Variation of LDR with Coefficient of friction between Sheet-Punch

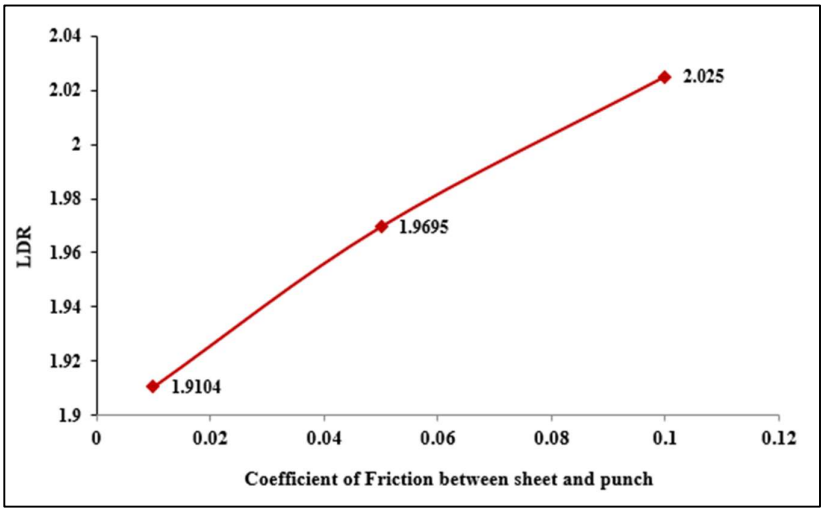

Figure.57: Variation of LDR with Coefficient of friction between sheet and Punch

The variation of LDR was plotted in Figure.57 with an increased coefficient of friction between sheet and punch. The coefficient of friction was taken as 0.01, 0.05, and 0.1, and the respective LDRs were found to be 1.9104,1.9695 and 2.025. It is observed the from that figure that high friction at the punch and cup interface leads to larger achievable LDRs.

4.9.7. Variation of LDR with Die corner radius

The variation of LDR was plotted in Figure.58 with an increase in die corner radius. The die corner radius was taken as 4, 6, and 8 with an increasing LDR of 1.9695, 1.9841, and 2.01. A

large die radius is preferred for decreasing the drawing load and increasing drawability. If the die radius is too small, a fracture can occur. However, the contact area between the blank holder and the flange becomes smaller with increasing die radius, which may result in wrinkles in the die radius region. The recommended values of die radii for aluminum alloys are about 4 to 8 blank thicknesses.

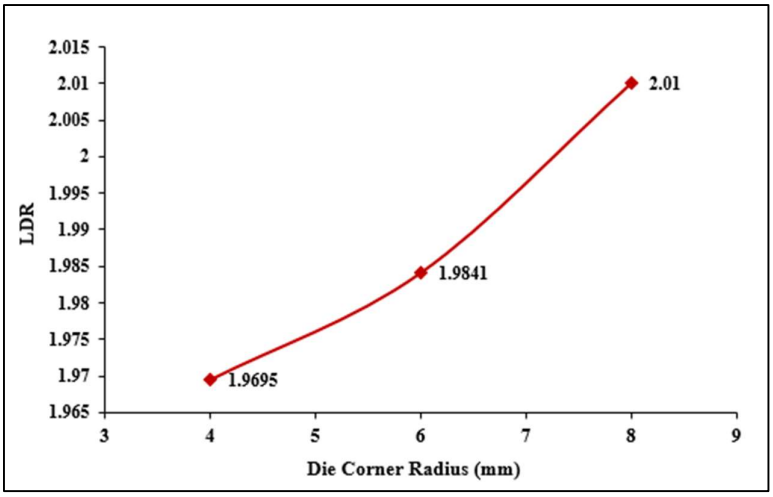

Figure.58: Variation of LDR with Die Radius

4.10. IDENTIFICATION OF JC PARAMETERS

4.10.1. Calculation of A, B and n parameter

The 0.2% offset line which is drawn to cuts the true stress vs true strain curve meets at point 'P' as seen in the Figure.59 Therefore, the value of 'A' will be 240.452 MPa that represent the yield stress of material at the location of deformation.

Now, after plotting the curve between '$\ln(\sigma - A)$ VS $\ln(\varepsilon)$' we will fit a trend line as seen in Figure.60 We will get y = 1.369x + 7.313 as equation of fit. The slope of the equation represents the n parameter i.e. 1.369. We got intercept equal to 7.313 which we have taken as ln(ε). Now we can get B parameter as following:

$$\ln(\varepsilon) = 7.313$$

Therefore the B value is found to be 1500.119 MPa

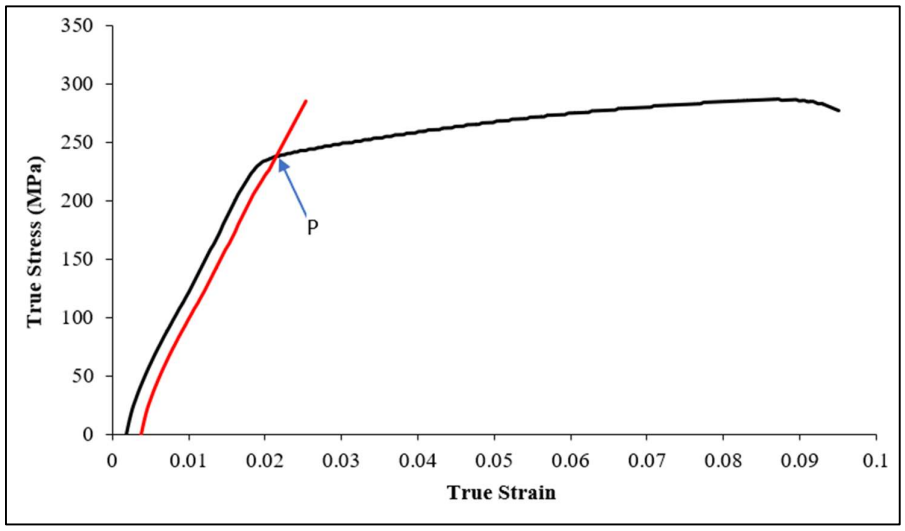

Figure.59: True stress vs True strain curve for determination of A parameter

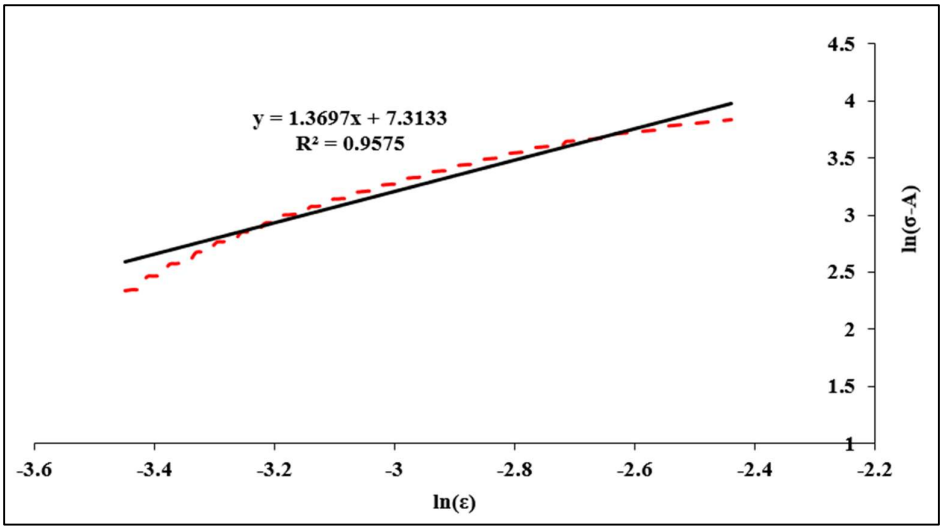

Figure.60: '$\ln(\sigma - A)$ VS $\ln(\varepsilon)$' curve to determine the B and n parameter

4.10.2. Calculation of C parameter

After plotting the curve between '$\frac{\sigma}{A+B(\varepsilon^{n})}$ vs $\ln \varepsilon^{*}$ we got the scatter plot as shown in the Figure.61 The plot is fitted with a trend line and the equation we got is y = 0.0093x + 1. The curve is forced intercept to 1. The slope of this curve is the 'C' parameter that is 0.0093.

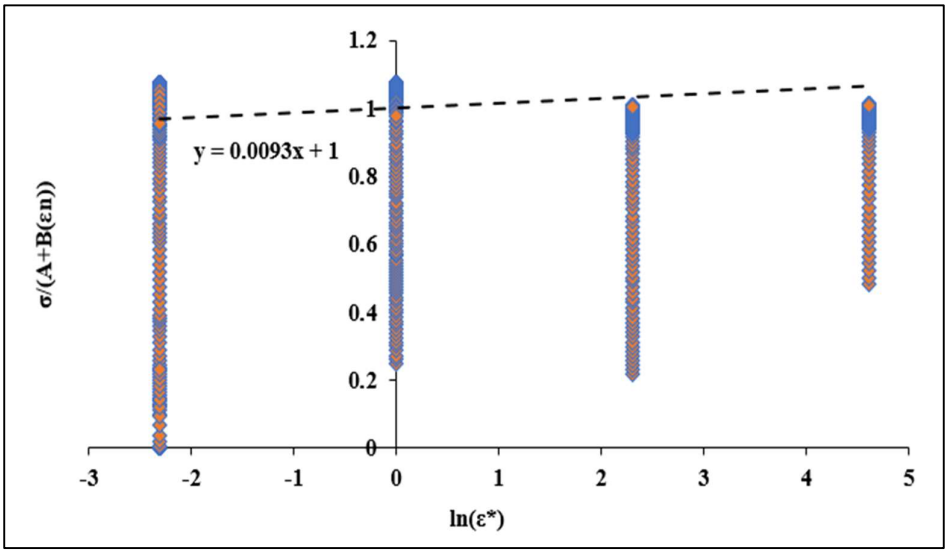

Figure.61: Scatter plot to determine the C parameter

4.10.3. Calculation of M parameter

Similar to the C parameter, M parameter is found. We will plot the scatter plot between '$\ln\left(1-\frac{\sigma}{A+B(\varepsilon^{n})}\right)$ vs $\ln(T^{*})$' and then add a trendline. The equation of trendline is y = 0.933x + 1 and the slope of this equation is 0.933 which gives us the M parameter as shown in Figure.62.

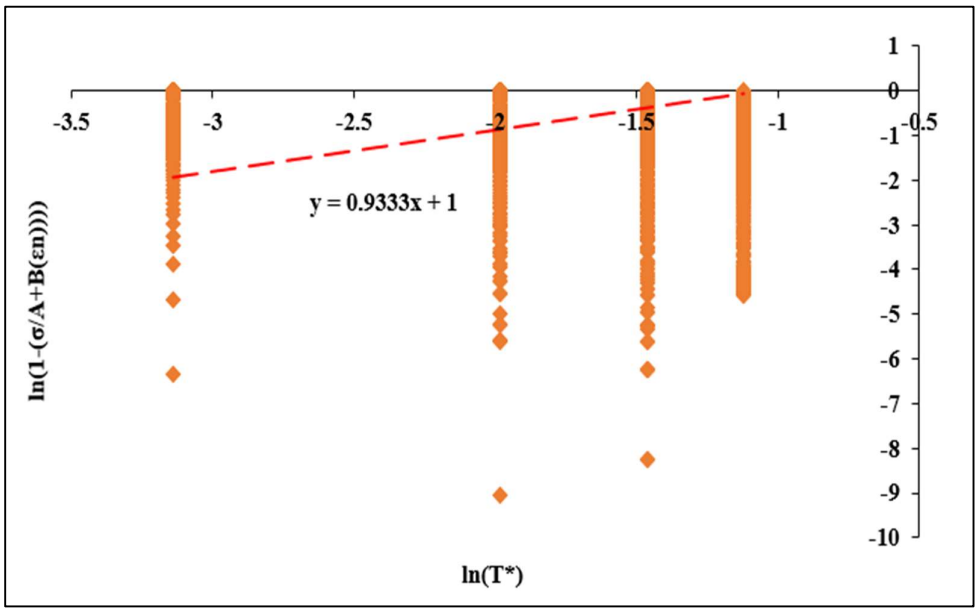

Figure.62: Scatter plot to determine the M parameter

Table.7: Material constants of Johnson-cook equation

Parameter	**A**	**B**	**n**	**C**	**M**
Value	240.452	1500.119	1.3697	0.0093	0.933

In conclusion the final Johnson-cook equation we obtain after substituting all the parameters is given in Eq.56:

$$\sigma_e = \left(240.452 + 1500.119\varepsilon_p^{1.3697}\right)\left(1 + 0.0093ln\frac{\dot{\varepsilon}}{\dot{\varepsilon_o}}\right)(1 - T^{*0.933}) \quad (56)$$

4.11. Drawability of AA6082 using Johnson cook model

The parameters and damage constants of Johnson-cook model are tabulated in Table.8 and Table.9. The material card for Johnson-cook model MAT_36 is shown in Figure 64.

Table.8: Parameters of Johnson-cook model

ρ (T/mm²)	**E (N/mm²)**	**G (N/mm²)**	**μ**	**C_P**
2.685e-09	6.895e+04	2.600e+04	0.33	9e+08

Table.9: Damage constants of Johnson-cook model [79]

D1	**D2**	**D3**	**D4**	**D5**
0.0164	2.2449999	-2.7980001	0.007	3.6500001

*MAT_JOHNSON_COOK_(TITLE) (015) (1)

	TITLE							
	AA6082							
1	MID	RO	G	E	PR	DTF	VP	RATEOP
	1	2.685e-09	2.600e+04	6.895e+04	0.3300000	0.0	0.0	0.0
2	A	B	N	C	M	TM	TR	EPSO
	240.45200	1500.1190	1.3697000	0.0093000	0.9330000	828.00000	298.00000	1.0000000
3	CP	PC	SPALL	IT	D1	D2	D3	D4
	9.000e+08	-1500.0000	2.0	0.0	0.0164000	2.2449999	-2.7980001	0.0070000
4	D5	C2/P	EROD	EFMIN	NUMINT			
	3.6500001	2.0000000	0	1.000e-06	0.0			

Figure.63: MAT_JOHNSON_COOK Material Card

The test was conducted for a sheet thickness of 1mm, sheet-die coefficient of friction of 0.1 and the punch diameter of 36mm. The blank diameter was varied and simulation of the model was used to determine the diameter where drawn cups are not tearing. At a blank diameter of 70.97mm, the drawn cups suffered fracture as shown in Fig.64 (a). But as diameter of blank to 70.96mm is decreased, cups were completely drawn as shown in Fig.64 (b) and hence this is the maximum diameter of the blank which is used to calculate LDR.

$$\text{LDR} = \frac{70.96}{36} = 1.971$$

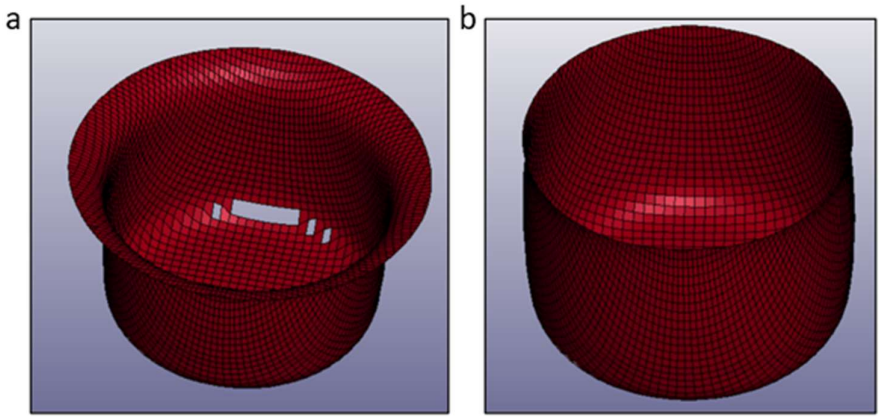

Figure.64: (a) Failure of sheet at radius of 70.97mm (b) Completely drawn cups at radius of 70.96mm

The cumulative effect of strain, strain rate, and temperature in the deep drawing operation was visualized by applying the Johnson-Cook model. The LDR value for Johnson-cook model was found to be 1.9711 which came out to be slightly better than the Barlat 3-parameter which gave

LDR as 1.96. So, the Johnson-Cook model is a robust model which can be applied at various temperatures and strain rate as it also considers the effect of strain rate and temperature effects on the material. It was seen that tearing of material in case of Johnson-Cook model was sudden because of high impact whereas in Barlat model, material experiences gradual necking and tearing.

CHAPTER 5

CONCLUSIONS

The main focus of this study was to study finite element analysis of the deep drawing model and its parameters. Different parameters such as blank position, speed, sheet thickness, clearances, coefficient of friction between die-sheet and punch-sheet, blank holding force, strain rate, temperature, etc. were varied and the drawability of the sheet was calculated. To take into consideration of anisotropic materials like AA6082, Barlat-3 parameters were used, and to visualize the combined effect of strain, strain rate, and temperature Johnson-Cook model was utilized in the Ls-Dyna PrePost (R) V4.6.17 material model characterization. The number of observations from the research findings were as follows:

- The results concluded that after annealing, the elongation was increased by 15% which was earlier in the range of 4-5% in case of non-annealed.
- The thickness in the flange region increased as the it experiences two opposite natures of stress, tensile in the radial direction and compressive in the circumferential direction.
- As the sheet thickness is decreased radial stress and compressive in the flange region of the deep-drawn sheet increases which results in wrinkling. The lesser the sheet thickness, the higher will be the radial and tangential compressive stress. To encounter the increased stresses, a higher amount of blank holding force is required to avoid wrinkling.
- With the increase in coefficient of friction there is decrease in sheet thickness at the wall section and if coefficient of friction is increased beyond a particular value, it will result in necking and eventually failure due to severe reduction in thickness.
- While finding drawability it was found that there was an increase in the LDR from 1.969 to 1.972 with the increase in sheet thickness of 1mm- 2mm as the load-carrying capacity of the material increases with sheet thickness.
- The LDR value is decreased with the increase in the punch speed. The numerical study shows LDR of 1.969, 1.965, and 1.959 at punch speed of 3000 mm/s, 4000mm/s, and 5000mm/s respectively.

- With the escalation in blank holding force from 5kN to 30 kN, there is decrease in the LDR from 2.037 to 1.6691. With less value of BHF, more material will be drawn in and deeper cups are drawn and the value of LDR increases.

- The friction also affects LDR between sheet-punch and sheet-die. With an increase in coefficient of friction between sheet and punch it was found that high friction at the punch and cup interface leads to larger achievable LDRs. It was also observed that with the increase in the coefficient of friction between sheet and die, LDR decreases. It can be inferred from the fact that as the friction between sheet and die is increased there is a resistance to motion. As the punch load increases the tendency to necking increases which lead to thinning on the wall of the cup hence drawability decreases.

- The die corner radius was taken as 4, 6, and 8 with an increasing LDR of 1.9695, 1.9841, and 2.01. A large die radius is preferred for decreasing the drawing load and increasing drawability.

- In isotropic material, the value of plastic strain ratio is 1 (width strain is equal to thickness strain) and in anisotropic material plastic strain ratio is less than 1. As a result, thinning resistance is more in isotropic material as compared to anisotropic materials. Thus, uniform thinning occurs in isotropic materials comparatively to anisotropic materials which will eventually lead to deeper cups. Moreover, in isotropic materials, planer anisotropy is zero, therefore, earings are not observed as compared to anisotropic material.

- The equation of Johnson-cook model was found to be

$$\sigma_e = \left(240.452 + 1500.119\varepsilon_p^{1.3697}\right)\left(1 + 0.0093ln\frac{\dot{\varepsilon}}{\dot{\varepsilon}_o}\right)(1 - T^{*0.933})$$

- The LDR value is found to be 1.9711 which came out to be slightly better than the Barlat 3-parameter which gave LDR as 1.96. So, the Johnson-Cook model is a robust model which can be applied at various temperatures and strain rate as it also considers the effect of strain rate and temperature effects on the material.

REFERENCES

[1] Z. Pater, “Cross-Wedge Rolling,” in *Comprehensive Materials Processing*, vol. 3, Elsevier Ltd, 2014, pp. 211–279. doi: 10.1016/B978-0-08-096532-1.00315-0.

[2] A. Alaswad, K. Y. Benyounis, and A. G. Olabi, “Optimization Techniques in Material Processing,” in *Reference Module in Materials Science and Materials Engineering*, Elsevier, 2016. doi: 10.1016/b978-0-12-803581-8.04004-2.

[3] Dorel Banabic, *Sheet Metal Forming Processes - Constitutive Modelling and Numerical Simulation*. 2010. doi: 10.1007/978-3-540-88113-1.

[4] M. Ramezani and Z. M. Ripin, “Introduction to sheet metal forming processes,” in *Rubber-Pad Forming Processes*, Elsevier, 2012, pp. 1–22. doi: 10.1533/9780857095497.1.

[5] R. Sousa, “Incremental Sheet Forming Technologies,” in *Reference Module in Materials Science and Materials Engineering*, Elsevier, 2016. doi: 10.1016/b978-0-12-803581-8.04055-8.

[6] M. S. Kulkarni and S. Y. Gajjal, “Review of Sheet Metal Forming Analysis,” 2015. [Online]. Available: www.internationaljournalssrg.org

[7] Gonfa Angasu and K. Srinivasulu Reddy, “Deep Drawing Process Parameters: A Review,” *International Journal of Current Engineering and Technology*, vol. Vol.6, no. No.4, Jan. 2016, doi: 10.14741/ijcet/22774106/6.4.2016.20.

[8] T. Taylan, A. Altan, A. A. E. Erman, and T. Tekkaya, *Sheet Metal Forming FUNDAMENTALS*, First. Ohio: ASM International, 2012. [Online]. Available: www.asrnwww.asminternational.orginternational.org

[9] M. Tisza, P. Zoltán Kovács, and Z. Péter Kovács, “NEW METHODS FOR PREDICTING THE FORMABILITY OF SHEET METALS,” *Journal of Production Processes and Systems*, vol. 6, no. 1, pp. 45–54, 2012, [Online]. Available: https://www.researchgate.net/publication/267243619

[10] S. A. J. Jahromi, A. Nazarboland, E. Mansouri, and S. Abbasi, “Investigation of formability of low carbon steel sheets by forming limit diagrams,” *Iranian Journal of Science & Technology, Transaction B, Engineering*, vol. 30, no. B3, 2006, [Online]. Available: www.SID.ir

[11] Z. Jiang, J. Zhao, and H. Xie, “Fundamentals of Microforming,” in *Microforming Technology*, Elsevier, 2017, pp. 3–27. doi: 10.1016/b978-0-12-811212-0.00001-7.

[12] E. Doege, T. Hallfeld, Y. Khalfalla, and K. Y. Benyounis, “Metal Working: Stretching of Sheets,” *Reference Module in Materials Science and Materials Engineering*, 2016, doi: 10.1016/b978-0-12-803581-8.03361-0.

[13] A. R. Joshi, K. D. Kothari, and R. L. Jhala, “Effects Of Different Parameters On Deep Drawing Process: Review,” *International Journal of Engineering Research & Technology (IJERT)*, vol. 2, no. 3, 2013, [Online]. Available: www.ijert.org

[14] A. I. O. Zaid, “Deep drawing mechanism, parameters, defects and recent results: State of the art,” in *IOP Conference Series: Materials Science and Engineering*, Sep. 2016, vol. 146, no. 1. doi: 10.1088/1757-899X/146/1/012009.

[15] D. Swapna, C. S. Rao, and S. Radhika, “A Review on Deep Drawing Process,” *International Journal of Emerging Research in Management and Technology*, vol. 6, no. 6, p. 146, Jun. 2018, doi: 10.23956/ijermt.v6i6.260.

[16] B. L. Juneja, N. Seth, and G. S. Sekhon, *Fundamentals of Metal Cutting and Machine Tools*, 2nd ed. New Age International, 2003.

[17] J. K. Pathak and V. Kumar Barnwal, “Analysis of Different States of Stress in Deep Drawing Process,” *IJSRSET*, vol. 2, no. 2, 2016, [Online]. Available: https://www.researchgate.net/publication/305357949

[18] George E. Dieter, *Mechanical Metallurgy*. McGraw-Hill, 1988. [Online]. Available: www.MechanicaLibrary.com

[19] Z. Marciniak, J. L. Duncan, and S. J. Hu, *Mechanics of sheet metal forming*. Butterworth-Heinemann, 2002.

[20] A. Jaisingh, K. Narasimhan, P. P. Date, S. K. Maiti, and U. P. Singh, “Sensitivity analysis of a deep drawing process for miniaturized products,” *Journal of Materials Processing Technology*, vol. 147, no. 3, pp. 321–327, Apr. 2004, doi: 10.1016/j.jmatprotec.2003.11.023.

[21] G. Behrens, F. O. Trier, H. Tetzel, and F. Vollertsen, “Influence of tool geometry variations on the limiting drawing ratio in micro deep drawing,” *International Journal of Material Forming*, vol. 9, no. 2, pp. 253–258, Apr. 2016, doi: 10.1007/s12289-015-1228-9.

[22] S. Hussaini, Singh SK, and Gupta AK, “Determination of the Limiting Drawing Ratio in Deep Drawing Process at Different Temperatures for Austenitic Stainless steel,” 2012. doi: 10.13140/2.1.1635.2640.

[23] R. Uday Kumar, “COMPARATIVE STUDY ON LIMITING DRAWING RATIO OF Al 1100 AND PURE COPPER,” vol. 11, 2020, [Online]. Available: www.jespublication.com

[24] A. I. O. Zaid and F. A. Hashim, “Effect of Punch and Die Profile Radii on Deep Drawing of Galvanized Steel,” *International Journal of Scientific & Engineering Research*, vol. 8, no. 1, 2017, [Online]. Available: http://www.ijser.org

[25] D.-K. Leu, “The limiting drawing ratio for plastic instability of the cup-drawing process,” 1999.

[26] R. Patel, H. Dave, and H. Raval, “Study of earing defect during deep drawing process with finite element simulation,” in *Key Engineering Materials*, 2015, vol. 639, pp. 91–98. doi: 10.4028/www.scientific.net/KEM.639.91.

[27] R. K. Saxena and P. M. Dixit, “Finite element simulation of earing defect in deep drawing,” *International Journal of Advanced Manufacturing Technology*, vol. 45, no. 3–4, pp. 219–233, Nov. 2009, doi: 10.1007/s00170-009-1963-5.

[28] B.V.S.Rao, P.V.R.Ravindra Reddy, G.Chandra Mohan Reddy, and G.Krishna Mohan Rao, “Optimization of Blank Holding Force in Deep Drawing of Cylindrical Cups Using Taguchi Approach,” *International Journal of Engineering and Innovative Technology(IJEIT)*, vol. 2, no. 3, 2012.

[29] R. Amaral, A. D. Santos, C. D. S. José, and S. Miranda, “Formability prediction for AHSS materials using damage models,” in *Journal of Physics: Conference Series*, May 2017, vol. 843, no. 1. doi: 10.1088/1742-6596/843/1/012018.

[30] Stuart Philip Keeler and Walter A. Backofen, “Plastic Instability And Fracture In Sheets Strechted OVer Rigid Punches,” MASSACHUSETTS INSTITUTE OF TECHNOLOGY, 1961.

[31] G. M. Goodwin, “Application of Strain Analysis to Sheet Metal Forming Problems in the Press Shop,” *SAE International*.

[32] S. K. Paul, “Theoretical analysis of strain- and stress-based forming limit diagrams,” *Journal of Strain Analysis for Engineering Design*, vol. 48, no. 3, pp. 177–188, Apr. 2013, doi: 10.1177/0309324712468524.

[33] A. O. Emmanuel, O. S. I. Fayomi, and I. G. Akande, “Aluminium Alloys as Advanced Materials: A short communication,” *IOP Conference Series: Materials Science and Engineering*, vol. 1107, no. 1, p. 012024, Apr. 2021, doi: 10.1088/1757-899x/1107/1/012024.

[34] C–H. Ng, S. N. M. Yahaya, and A. A. A. Majid, “Reviews on aluminum alloy series and its applications,” *Academia Journal of Scientific Research*, vol. 5, no. 12, pp. 708–716, 2017, doi: 10.15413/ajsr.2017.0724.

[35] J.R. Davis, “Alloying: Understanding the Basics,” *ASM International*, pp. 351–416, 2001, doi: 10.1361/autb2001p351.

[36] I. A. B. Magno *et al.*, “Effect of the T6 heat treatment on microhardness of a directionally solidified aluminum-based 319 alloy,” in *Materials Research*, 2017, vol. 20, pp. 667–675. doi: 10.1590/1980-5373-mr-2016-0961.

[37] O. Prach, J. Hornik, and K. Mykhalenkov, “Effect of the addition of Li on the structure and mechanical properties of hypoeutectic Al-Mg2Si alloys,” *Acta Polytechnica*, vol. 55, no. 4, pp. 253–259, Sep. 2015, doi: 10.14311/AP.2015.55.0253.

[38] I. Z. Awan and A. Q. Khan, “Recovery, recrystallization, and grain-growth,” *Journal of the Chemical Society of Pakistan*, vol. 41, no. 1, pp. 1–42, 2019, doi: 10.52568/000707/jcsp/41.01.2019.

[39] W. F. Hosford and R. M. Caddell, *Metal forming : mechanics and metallurgy*. Cambridge University Press, 2007.

[40] F. Barlat and J. Lian, “PLASTIC BEHAVIOR AND STRETCHABILITY OF SHEET METALS. PART h A YIELD FUNCTION FOR ORTHOTROPIC SHEETS UNDER PLANE STRESS CONDITIONS,” *International Journal ofPlastic#y*, vol. 5, pp. 51–66, 1989.

[41] S. Jurendić and S. Gaiani, “Deep drawing simulation of α-titanium alloys using LS-Dyna,” May 2011.

[42] G. R. Johnson and W. H. Cook, “A CONSTITUTIVE MODEL AND DATA FOR METALS SUBJECTED TO LARGE STRAINS, HIGH STRAIN RATES AND HIGH TEMPERATURES.”

[43] H. Zhao, “A constitutive model for metals over a large range of strain rates Identification for mild-steel and aluminium sheets,” *Materials Science and Engineering* , pp. 95–99, 1997.

[44] Y. C. Lin, X. M. Chen, and G. Liu, “A modified Johnson-Cook model for tensile behaviors of typical high-strength alloy steel,” *Materials Science and Engineering A*, vol. 527, no. 26, pp. 6980–6986, Oct. 2010, doi: 10.1016/j.msea.2010.07.061.

[45] S. Reddy, S. Rajesham, and P. R. Reddy, “Evaluation of Limiting Drawing Ratio (LDR) in Deep Drawing by Rapid Determination Method,” 2014. [Online]. Available: http://inpressco.com/category/ijcet

[46] F. Pourboghrat, S. Venkatesan, and J. E. Carsley, “LDR and hydroforming limit for deep drawing of AA5754 aluminum sheet,” *Journal of Manufacturing Processes*, vol. 15, no. 4, pp. 600–615, Oct. 2013, doi: 10.1016/j.jmapro.2013.04.003.

[47] B. Patil and B. S. Kodli, “Simulation Study on Effect of Punch Velocity in Single Stage Deep Drawing Process Using AFDEX Software,” 2021. [Online]. Available: www.ijsrd.com

[48] M. T. Browne and M. T. Hillery, “Optimising the variables when deep-drawing C.R.1 cups,” *Journal of Materials Processing Technology 136*, pp. 64–71, 2003.

[49] R. Sridhar and S. ShankarC, “Review On Micro Deep Drawing Process For Thin Foil Materials,” *International Journal of Innovations in Engineering and Technology (IJIET)*, vol. 11, 2018, doi: 10.21172/ijiet.113.03.

[50] S. K. Singh, K. Mahesh, A. Kumar, and M. Swathi, “Understanding formability of extra-deep drawing steel at elevated temperature using finite element simulation,” *Materials and Design*, vol. 31, no. 9, pp. 4478–4484, Oct. 2010, doi: 10.1016/j.matdes.2010.04.049.

[51] L. Tian, C. Men, and Q. Yu, “Optimization of Process Parameters in Deep Drawing Process Based on Orthogonal Experiment Method,” 2015.

[52] T. Altinbalik and A. Tonka, “NUMERICAL AND EXPERIMENTAL STUDY OF SHEET THICKNESS VARIATION IN DEEP DRAWING PROCESSES,” *International Journal of Modern Manufacturing Technologies*, vol. IV, no. 2, pp. 2067–3604, 2012.

[53] A. Shaaban and A. S. Elakkad, “Numerical and experimental analysis of single-acting stroke deep drawing of symmetric low-depth products without blank holder,” *Ain Shams Engineering Journal*, vol. 12, no. 3, pp. 2907–2919, Sep. 2021, doi: 10.1016/j.asej.2020.11.015.

[54] A. Chennakesava Reddy, “Study on Deep Drawing Process Parameters - A Review,” *International Journal of Scientific & Engineering Research*, vol. 7, no. 6, 2016, [Online]. Available: http://www.ijser.org

[55] J. N. Mistri, K. D. Kothari, and G. K. Sharma, “Experimental and Simulation study of Deep drawing process-A review,” *International Journal of Advance Engineer ing and Research Development (IJAERD)*, vol. 1, no. 6, pp. 2348–4470, 2014.

[56] D. Pan, G. Zhang, H. Xie, • Fanghui Jia, H. Kamali, and Z. Jiang, “Effects of forming velocity on micro deep drawing performance with different blank thickness.”

[57] G. Ramesh, G. Chandra, and M. Reddy, “Analysis of Optimization of Blank Holding Force In Deep Drawing By Using LS DYNA,” vol. 3, pp. 1975–1995, [Online]. Available: www.ijera.com

[58] M. Jain, J. Allin, and M. J. Bull, “Deep drawing characteristics of automotive aluminum alloys,” *Materials Science and Engineering*, vol. 256, pp. 69–82, 1998.

[59] G. G. Niranjan and U. Chakkingal, “Deep drawability of commercial purity aluminum sheets processed by groove pressing,” *Journal of Materials Processing Technology*, vol. 210, no. 11, pp. 1511–1516, Aug. 2010, doi: 10.1016/j.jmatprotec.2010.04.009.

[60] Y. gen WANG *et al.*, “Influence of blank holder type on drawability of 5182-O aluminum sheet at room temperature,” *Transactions of Nonferrous Metals Society of China (English Edition)*, vol. 26, no. 5, pp. 1251–1258, 2016, doi: 10.1016/S1003-6326(16)64225-5.

[61] E. T. Harpell, M. J. Worswick, M. Finn, M. Jain, and P. Martin, “Numerical prediction of the limiting draw ratio for aluminum alloy sheet,” *Journal of Materials Processing Technology 100*, pp. 131–141, 2000.

[62] N. Kotkunde, A. D. Deole, A. K. Gupta, and S. K. Singh, “Experimental and numerical investigation of anisotropic yield criteria for warm deep drawing of Ti-6Al-4V alloy,” *Materials and Design*, vol. 63, pp. 336–344, Nov. 2014, doi: 10.1016/j.matdes.2014.06.017.

[63] R. Lostado-Lorza, S. Iñiguez-Macedo, I. Eguía-Cambero, E. Fraile-García, and J. Ferreiro-Cabello, “Aluminium sheet drawing cold process considering anisotropic behavior in Finite Element Analisys. Sheet metal process considering planar anisotropy and Barlat’s yield function,” in *Proceedings of The 5th Virtual Multidisciplinary Conference*, Dec. 2017, vol. 5, pp. 157–159. doi: 10.18638/quaesti.2017.5.1.331.

[64] Y. Marumo, H. Saiki, and L. Ruan, “Effect of sheet thickness on deep drawing of metal foils Manufacturing and processing,” *Journal of Achievements and Manufacturing Engineering*, vol. 20, no. 1–2, 2007.

[65] H. S. Kim, M. Koç, J. Ni, and A. Ghosh, “Finite element modeling and analysis of warm forming of aluminum alloys - Validation through comparisons with experiments and determination of a failure criterion,” *Journal of Manufacturing Science and Engineering, Transactions of the ASME*, vol. 128, no. 3, pp. 613–621, Aug. 2006, doi: 10.1115/1.2194065.

[66] D. Rajput, A. Singh, and S. Kumar, “Evaluation of Johnson-Cook Material Model Parameters of AA6063-T6,” *International Research Journal of Engineering and Technology*, 2020, [Online]. Available: www.irjet.net

[67] S. Khare, K. Kumar, S. Choudhary, P. K. Singh, R. K. Verma, and P. Mahajan, “Determination of Johnson–Cook Material Parameters for Armour Plate Using DIC and FEM,” *Metals and Materials International*, vol. 27, no. 12, pp. 4984–4995, Dec. 2021, doi: 10.1007/s12540-020-00895-3.

[68] S. Li, J. Sui, F. Ding, S. Wu, W. Chen, and C. Wang, “Optimization of Milling Aluminum Alloy 6061-T6 using Modified Johnson-Cook Model,” *Simulation Modelling Practice and Theory*, vol. 111, Sep. 2021, doi: 10.1016/j.simpat.2021.102330.

[69] G. Wang, X. Li, G. Yu, and Z. Gu, “Hot deformation characteristics and processing maps of AA7075-H18 alloy sheet under hot forming process conditions,” *Materials Letters*, vol. 321, p. 132413, Aug. 2022, doi: 10.1016/J.MATLET.2022.132413.

[70] R. Seddik *et al.*, “Identification of constitutive equations at very high strain rates using shock wave produced by laser,” *European Journal of Mechanics - A/Solids*, vol. 92, p. 104432, Mar. 2022, doi: 10.1016/J.EUROMECHSOL.2021.104432.

[71] M. Hao, Q. Yu, C. Wei, Y. Chen, L. Chai, and Y. Ge, “Statistical Determination of Johnson-Cook Model Parameters for Porous Materials by Machine Learning and Particle Swarm Optimization Algorithm,” *Journal of Materials Engineering and Performance*, Apr. 2022, doi: 10.1007/s11665-022-06765-w.

[72] S. Deb, A. Muraleedharan, R. J. Immanuel, S. K. Panigrahi, G. Racineux, and S. Marya, "Establishing flow stress behaviour of Ti-6Al-4V alloy and development of constitutive models using Johnson-Cook method and Artificial Neural Network for quasi-static and dynamic loading," *Theoretical and Applied Fracture Mechanics*, vol. 119, p. 103338, Jun. 2022, doi: 10.1016/J.TAFMEC.2022.103338.

[73] W. Moćko and Z. Kowalewski, "DYNAMIC PROPERTIES OF ALUMINIUM ALLOYS USED IN AUTOMOTIVE INDUSTRY," *Journal of KONES. Powertrain and Transport*, vol. 19, no. 2, pp. 345–351, Jan. 2015, doi: 10.5604/12314005.1138222.

[74] "Aluminium-Alloys-Aluminium-6082-Properties-Fabrication-and-Applications," 2005, Accessed: May 07, 2022. [Online]. Available: https://www.azom.com/article.aspx?ArticleID=2813

[75] LIVERMORE SOFTWARE TECHNOLOGY CORPORATION (LSTC), *LS-DYNA KEYWORD USER'S MANUAL Volume I*. 1992. [Online]. Available: www.lstc.com

[76] LSTC, "LS-DYNA ® KEYWORD USER'S MANUAL VOLUME II Material Models," 1992. [Online]. Available: www.lstc.com

[77] W. Song, J. Ning, X. Mao, and H. Tang, "A modified Johnson–Cook model for titanium matrix composites reinforced with titanium carbide particles at elevated temperatures," *Materials Science and Engineering A*, vol. 576, pp. 280–289, Aug. 2013, doi: 10.1016/j.msea.2013.04.014.

[78] B. Song and B. Sanborn, "A Modified Johnson-Cook Model for Dynamic Response of Metals with an Explicit Strain-and Strain-Rate-Dependent Adiabatic Thermosoftening Effect."

[79] Adekanmi Miracle Adeyinka and Mesach O. Olaleke, "Predictive Model for Thermal Response During Dry Machining of Al 6082-T6 using Fem," *Article in International Journal of Engineering and Technical Research*, vol. 9, no. 6, Jun. 2020, [Online]. Available: https://www.researchgate.net/publication/342661400